Spring 4-30-2020

Spectroscopic and Computational Studies of the Agricultural Active Ingredient Dicamba

James Johnson

Spectroscopic and Computational Studies of the Agricultural Active Ingredient Dicamba

By: James “Trip” Johnson

A thesis submitted to the faculty of The University of Mississippi in partial fulfillment of the requirements of the Sally McDonnell Barksdale Honors College.

Oxford, MS
May 2020

Approved by:

_____

Dr. Nathan I. Hammer
Advisor

_____

Dr. James Cizdziel
Reader

_____

Dr. Susan Pedigo
Reader

Acknowledgements

When I stepped on this campus four years ago, I would have never guessed how hard it would be to say good-bye to this place. The University of Mississippi has provided me with a platform to be supported and succeed in every endeavor that I pursue. This University has become my home away from home. I am so thankful I made the decision in choosing the University of Mississippi four years ago. This place has challenged me, molded me, and changed me for the better. It has given me mentors, friends, and relationships that will last a lifetime. I will forever be indebted to the University of Mississippi.

I first would like to thank my family for their endless support. They have provided me with a support system that has allowed me achieve whatever I set my mind to. I next want to thank Dr. Hammer for allowing me to work his research group. His constant guidance helped me finish this project and be proud of the work I have done. I would like to thank the graduate students of the Hammer Group for their help when I needed it. Their willingness to answer my perpetual questions helped me make significant progress throughout this journey. To my friends, I could not have done college without you. Your never-ending support and constant encouragements at the right times meant far more than I could express. My last thank you goes to the Sally McDonnel Barksdale Honors College. Words do not do enough justice the impact this group of staff and students has had on my college experience. My time at the University of Mississippi would not be the same without it. The Honors College provided me with a home and a family I could not have found anywhere else on this campus. I have grown as both a student and an individual because of the lessons I learned during my journey as a member of the SMBHC.

This journey is one I did not realize would come to a close as fast as it did. I could have never guessed how much one place could impact me. This place and the people within it are the reason these past four years have gone by so fast. I am forever changed by the people, places, and moments of the last four years.

Spectroscopic and Computational Studies of the Agricultural Active Ingredient Dicamba

James “Trip” Johnson (Under the direction of Dr. Nathan Hammer)

3,6-dichloro-2-methoxy benzoic acid, more commonly known as Dicamba, is the active ingredient in an array of pesticides used on farmlands across the globe. Dicamba’s mode of action works by mimicking the plant hormone auxin, which is synonymous to growth hormones in mammals. The mimicking of auxin results in excessive elongation and growing, which is eventually fatal for plants when the rate of growth can no longer be sustained. Dicamba has risen in prominence in recent years due to drift damage as a result of Dicamba’s high volatility. Having the ability to identify Dicamba is crucial for the agricultural industry. The purpose of this experiment was to study intermolecular interactions involving Dicamba using Raman Spectroscopy and computational chemistry, since there has not been any Raman spectrum, experimental or theoretical, referenced or taken. In this study, both theoretical and experimental Raman spectra were acquired. In addition, theoretical water calculations were studied, and the lowest-energy conformations for systems with one and two water molecules were found. These water calculations showed red shifts or decreases in energy for carbonyl and O-H stretching vibrational modes.

Table of Contents

List of Figures and Tables

Figures

Tables

Chapter 1: The History of Pesticides and Dicamba

A pesticide is a broad term that encompasses many chemical variations with the intention of eliminating unwarranted pests. Pesticides most commonly refer to herbicides, insecticides, and fungicides. Of these, herbicides are by far the most common, being used on approximately 80% of the current crop total in the United States[1,2]. In addition, herbicides account for 40% of the global pesticide usage with the United States accounting for over half the amount[1,2]. The Food and Agriculture Organization defines a pesticide as: any substance or mixture of substances intended for preventing, destroying or controlling any pest, including vectors of human or animal disease, unwanted species of plants or animals, causing harm during or otherwise interfering with the production, processing, storage, transport, or marketing of food, agricultural commodities, wood and wood products or animal feedstuffs, or substances that may be administered to animals for the control of insects, arachnids, or other pests in or on their bodies[3]. Pesticides are classified based on the organisms being targeted. For example, insecticides target insects and fungicides target fungi. For herbicides, there are various ways they can be classified. Chemical name, toxicity, chemical compound characteristics are just a few of the many[4]. One of the more predominant ways to classify herbicides is based on the mode of action of the chemical. A mode of action is the mechanism in which a substance causes an anatomical change on an organism. Most modes of action for pesticides look at the effects caused on the tissue or cellular level. Modes of action are used to group together related

active ingredients[5]. The main ingredient in related pesticides may not be the same, but the injury pattern and translocation pattern throughout the plants will be similar. Mode of action classification is broken into two categories: contact herbicides and translocated herbicides. Contact herbicides affect only the regions of the plant the herbicide comes in contact with. There is minimal absorption by foliage or roots. As a result, sufficient amounts of contact herbicides have to be applied for the herbicide to be effective. Examples of contact herbicides include paraquat and diclofop[6]. In contrast, translocated herbicides are systemic herbicides, meaning once absorbed by foliage and roots, the chemical compounds in the herbicide translocate throughout the entire plant and disrupt physiological significant biochemical pathways. Examples of translocated herbicides include glyphosate, atrazine, and 2,4-D[6].

In the paper, herbicides will primarily be analyzed. Herbicides have a plethora of uses ranging from agricultural purposes to urban uses. The uses of herbicides have changed for centuries, going all the way back to the first use of pesticides. Key developments throughout scientific history have led to revelations in the pesticide market.

1A: History of Pesticides

Since the beginning of food cultivation, there has always been a desire to increase crop output. This urge to produce more food has led mankind to discover and eventually enhancing multiple ways to increase crop yields. These developments have led to the pesticides used in the present. The first known utilization of pesticides to better crop yields occurred around 2500 B.C[7]. This was done in ancient Sumerian culture where elemental

sulfur dusting was used. In ancient Mesopotamia, elemental sulfur was used to control powdery mildew on fruit trees. This use of sulfur is also seen in ancient Greece[7].

The next major evolution of pesticides occurred during the fifteenth century. Inorganic pesticides containing lead, mercury, and arsenic were introduced and became the primarily used pesticides to kill pests. Each of these element-based pesticides displayed different modes of action to decrease pest populations. Lead-based pesticides served as a calcium analog and resulted in the incomplete formation of heme. This incomplete formation of heme results in anemia, which is a deficiency in red blood cells or hemoglobin in the blood[8]. Mercury-based pesticide contains mercury oxide molecules, which interact with thiols to stop enzymatic activities[8]. Arsenic-based pesticides used during this time period contain arsenic (III) oxides that interact with cysteine and Coenzyme A, which disrupts enzymatic pathways, specifically the production of ATP[8].

These pesticides rose in prevalence because of their ability to last far longer in the environment than previously used pesticides. This long-lasting property is the result of these pesticides not degrading easily after spraying applications[8]. Though the impact of these pesticides increased crop yields, the fact that these inorganic pesticides stayed in the environment for longer periods of time meant the wildlife and people in the areas suffered from the toxicity of these pesticides. With time, these pesticides reached groundwater and other ecosystems since the degradation process was so slow, eventually leading to a phenomenon called leaching[8]. Leaching is the movement of contaminants, main pesticides in water, through permeable soil[8]. Leaching is not a major issue for pesticides that degrade easily once sprayed. For the lead, mercury, and arsenic-based pesticides, however, leaching grew common due to the resilience to degradation[8].

The seventeenth century saw the introduction of the scientific method. This new procedure ushered in new approaches for scientific observation and experimentation. The new sense of scientific inquiry translated to the advent of pesticide usage in European countries[9]. A large range of new pesticides was introduced during this time of heightened experimentation because travel across the globe increased. This allowed for various types of pesticides derived from multiple materials to be experimented with and the results observed. Many of the pesticides deemed successful by the new measures of experimentation derived from tobacco. Tobacco contains nicotine sulfate which is highly toxic. This high toxicity was intended to kill sucking insects such as aphids, spider mites, and thrips. The nicotine sulfate in these pesticides disrupted pathways with the nervous systems of these insects, eventually leading to the death of these insects. Tobacco-based pesticides rose in prominence because of their decimating impact on the targeted insects. The issue, however, is that the toxicity of nicotine sulfate also negatively affects people, pets, and beneficial insects. For this reason, tobacco-based pesticides were never commercially produced. Synthetic pesticides mimicking the effects of nicotine sulfate have been created to get the same effects[9].

The nineteenth-century marked the beginning of manufactured chemical pesticides. These chemicals were being extracted from their botanical source and purified in laboratories for the first time. Throughout the century, various chemicals were extracted and purified from different plants and anatomical components of plants. Some of these included pyrethrins which were extracted from flowering plants, cyanides came from the pits of some fruits, and rotenone was isolated from plant roots[10]. During the period, chemical mixtures intended for pesticides were put under the scientific method throughout

the entire formulation process for the first time. This testing and experimentation led to the commercial production of pesticides[10].

The twentieth century went through periods of time with different pesticides dominating the market. The later stages of the nineteenth and early part of the twentieth century saw the refining of pest control, which before this time had only been used for simple procedures and cases. The early synthetic organic pesticides paved the way for the first modern synthetic pesticides, which were comprised of organochloride compounds[11]. This change in synthetic pesticides was primarily initiated by World War II. Dichlorodiphenyltrichloroethane (DDT) became the Allied Forces pesticide of choice because there were limited supplies of flowers from the genus *Chrysanthemum*. This genus of flowers was the main source of pyrethrin extract, which was one of the main chemicals in pesticides at the time. With pyrethrin-based pesticides not in abundance, DDT was the primary pesticides used during the war with the purpose to kill insects serving as vectors for typhus, malaria, and dengue fever[12].

The overreliance of pesticides during the war led to the 1940s and 1950s being labeled as the beginning of the "Pesticide Era". After the war, DDT was commercially available for agricultural applications. The commercialization of this insecticide quickly led to excessive dependence throughout the entire agricultural industry. The first signs of DDT resistance among insects appeared in the 1950s, leading to the search for new insecticides[13]. DDT resistance was compounded with the fear of the insecticide's toxicity being so extreme that wildlife other than insects would be negatively affected, upsetting ecosystems' biodiversity[14].

Also during the twentieth century, the first modern herbicide was discovered. 2,4-Dichlorophenoxyacetic acid, usually referred to as 2,4-D, spurred the shift from primarily inorganic herbicides to organic ones. This shift was highly supported by environmental proponents due to the excessively long period of time needed to break down inorganic pesticides. 2,4-D was discovered simultaneously in both the United States and the United Kingdom[15]. In 1940, W.G. Templeman, a British chemist, showed that certain synthetic growth substances applied to weeds kill the pest while maintaining the cereal crop affected by the weeds. A year later, Templeman and team synthesized 2,4-D. Robert Pokorny synthesized the molecule the same year in the United States[15].

Juda Hirsch Quastel, a British-Canadian biochemist, made similar discoveries and was able to independently synthesize 2,4-D as well. In addition to synthesizing the molecule, Quastel was able to quantize the various plant hormones, inhibitors, and microorganisms that have a direct impact on plant growth[16]. Quastel's research on effectors of plant growth and the development of 2,4-D led to the commercialization of 2,4-D-based pesticides in 1946. The addition of this herbicide to the market was a major revolution in the agricultural industry. 2,4-D was the first successful selective herbicide[16]. This allowed for crop yields to increase drastically because specific weeds could be targeted. 2,4-D works by mimicking plant growth hormones, leading to uncontrolled growth and eventual death. It is in the same class of pesticides as Dicamba, the main topic of this paper. The impact of the 2,4-D introduction into the market can still be felt in the present time. 2,4-D is still one of the most commonly used herbicides[16].

Triazine family of pesticides was discovered in the 1950s. This family is most notable for atrazine. Atrazine targets both pre- and post-emergent broadleaf weeds[17]. It is

applied mainly to lawns and golf course turf. Atrazine is commonly known for its inability to break down in nature as fast as other organic herbicides. This slow break down results in groundwater contamination. Atrazine has been found in drinking water in certain areas of the United States and has been criticized by the Environmental Protection Agency[17].

1B: Glyphosate and Genetically Modified Organisms

Glyphosate, or N-(phosphonomethyl) glycine, was discovered by Monsanto chemist John E. Franz in 1970. Upon the discovery of glyphosate, Monsanto patented a glyphosate-based herbicide called Roundup in 1974, leading Monsanto to the pinnacle of the pesticide market. After the advent of glyphosate, the United States witnessed a 100 fold increase of glyphosate-based herbicides from 1970 to 2016. The introduction of Roundup and other glyphosate products led to the development of glyphosate-resistant weeds, which will be examined in further detail later[18,19].

Glyphosate-based herbicides mainly target annual broadleaf weeds and grasses competing with crops. Glyphosate is sprayed post emergence, meaning the pesticide is applied after the seedling sprouts from the seed. This is done because glyphosate is primarily absorbed through the foliage of the plant. The roots cannot absorb glyphosate because the molecules become so tightly bound to the soil, not allowing the molecule to become mobile and reach the roots[20]. Once absorbed, glyphosate is transported throughout the plants to various key growing points. With glyphosate only absorbing through the leaves, pre-emergent plants, plants that have not sprouted yet, will not be impacted by the glyphosate because there are no leaves to absorb the chemical. Glyphosate is also a non-

selective herbicide, meaning it kills most plants sprayed with glyphosate-based products. Due to this, many crops have been genetically engineered to resist glyphosate[20].

Glyphosate's mode of action inhibits key enzymes in the shikimate pathway. This biosynthetic pathway is used by many organisms such as bacteria, fungi, and plants. It is not found in animals. This pathway leads to the formation of aromatic amino acids. Glyphosate disrupts this pathway by inhibiting the enzyme 5-enolpyruvylshikimate-3-phosphate synthase. This enzyme occurs at the sixth step of the biosynthesis pathway. This step is responsible for converting shikimate-3-phosphate and phosphoenolpyruvate to 5-enolpyruvylshikimate-3-phosphate. This is the targeted enzyme because this is the final major reaction before the creation of aromatic amino acids. This pathway is targeted because aromatic amino acids serve as precursors for hormones and critical metabolites needed for plant development[21].

Glyphosate is the most widely used pesticide across the globe. Its success is a direct result of its effectiveness compared to other pesticides when glyphosate was first introduced. Glyphosate-based pesticides helped farmers complete jobs at faster rates. This pesticide could be applied to crops and weeds post-emergent. Weather conditions never were an issue. If the proper spraying time was missed for a particular herbicide, glyphosate could be sprayed directly on large weeds, reducing the invasive pests from fields. Glyphosate also is relatively inexpensive compared to other pesticides. This was also compounded by its potency[22]. Before glyphosate, farmers had to mix multiple pesticides together to achieve a strong dose of the chemical. The advent of glyphosate meant farmers saved money using a cheaper pesticide while also saving money using fewer pesticides since they were not needed to mix with glyphosate. The final major benefit that made

glyphosate an instant success was its environmental advantages over other pesticides. Glyphosate was less toxic than most other pesticides on the market at the time of its introduction. Being less toxic, glyphosate could not damage newly planted crops once it reached the soil. This low toxicity allowed farmers to practice no-tillage farming. Farmers till soil to mix organic molecules together and kill weeds after a harvest period. Tillage also occurs to breakdown residues from pesticides that still persist in the soil. The disadvantage of tilling soil is the integrity of soil is disrupted. This leads to the soil not being able to conserve as much water as non-tilled soil. With glyphosate not being as toxic, there is no need to breakdown residue with soil tillage, which has been shown to better water retention in soil and higher crop yields[22].

As mentioned earlier, Monsanto trademarked glyphosate as Roundup. This commercialization quickly led to high concentrations of Roundup usage in both agricultural and urban settings. The major issue, though, was glyphosate-based pesticides were non-selective, meaning the glyphosate did not target one particular weed or plant species, any plant sprayed with glyphosate would be negatively impacted[23].

As a result of glyphosate's non-selective nature, new mechanisms were experimented with to find ways to maintain glyphosate's effects on weeds and invasive species while not decimating crop yields. The new mechanism that turned out to be the most successful was the creation of genetically modified organisms (GMOs). GMOs are an organism whose genetic material has undergone genetic engineering to obtain a desired characteristic or trait[23]. In regards to glyphosate, crops have been genetically engineered to withstand the effects of glyphosate, meaning that glyphosate's non-selective properties will not hurt glyphosate-resistant crops[23]. This new development was first seen in 1994 when

the United States commercially approved the selling of Roundup Ready soybeans. The commercial launch of Roundup Ready soybeans occurred in 1996. This allows farmers to control pest plants with Roundup will never endanger the soybeans. The introduction of Roundup Ready soybeans quickly grew at unprecedented rates. Before long, additional crops such as corn, canola, alfalfa, cotton, and wheat soon were genetically engineered to also be glyphosate-resistant. This constant growth of new crops being glyphosate-resistant took hold throughout the entire American agricultural industry[24]. As of 2015, certain crop outputs throughout the United States are overwhelmingly genetically modified; these crops include corn and cotton production being 89% genetically modified and soybeans being 94% genetically modified. The United States accounts for 59% of the world's GMO crop output. This large shift to GMOs resulted in glyphosate-pesticide consumption also increasing at an unprecedented rate[24]. This overreliance has led to 29 weed species worldwide that are resistant to glyphosate. The development of these glyphosate-resistant weeds led to farmers experiencing lower crop yields[25]. As a result, farmers had to shift to other pesticides to account for these newly resistant weeds.

1C: Dicamba

Dicamba, the main focus of this paper, has gone in and out of popularity since its approval in 1962. Dicamba's most recent rise in prominence is due to the appearance of multiple glyphosate-resistant weeds persisting on farms. This surge in attention for Dicamba came from the development of Dicamba-resistant soybeans. This technology was created to combat the issue of pesticide-resistant weeds. Scientists hoped the introduction

of this new technology will prevent the development of many more resistant weeds, leading to an increase in crop yields.

Dicamba Development and History

Dicamba, or 3,6-dichloro-2-methoxy benzoic acid, is an active ingredient in pesticides that acts as an auxin mimicker. Dicamba is a phenoxy herbicide family. The growth-enhancing properties of this family were first described in the early 1940s. The discovery of Dicamba occurred in the United Kingdom in 1958 at Jealott's Hill Experimental Station. Scientists Zimmerman and Hitchcock were the individuals who made the discovery. Its usage was approved in 1962 following the patent of the molecule by Velsicol Chemical Corporation[26]. In the years to come following the patent approval, new variations of Dicamba herbicides were approved by the United States Department of Agriculture (USDA). In 1964, Banvel herbicide contained a formulation of Dicamba with dimethylamine. A few decades later, Marksman created a version of Dicamba in combination with potassium[26].

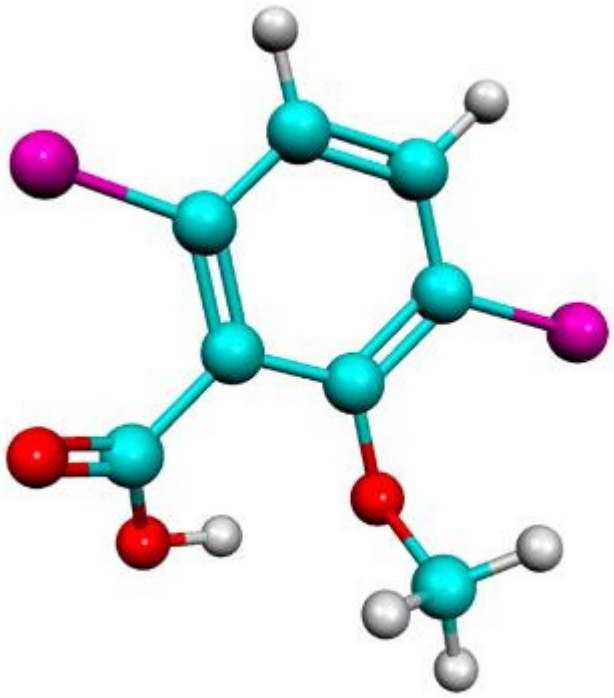

Figure 1.1: 3,6-dichloro-2-methoxy benzoic acid

The next major headlines containing Dicamba occurred in 2005. Monsanto licensed a Dicamba-resistant trait that was developed at the University of Nebraska. This trait came from the use of a bacterial gene Dicamba monooxygenase (DMO), which encodes a Rieske non-heme monooxygenase[27]. The enzyme inactivates Dicamba when it is in the nuclear genome or chloroplast of transgenic plants. DMO enzymes destroy Dicamba herbicide before the lethal effects disrupt plant growth, allowing the plants with this bacterial gene to withstand Dicamba-based herbicides[27]. The Environmental Protection Agency (EPA) approved this trait the following year. The development of Dicamba-resistant traits soon led to a resurgence of Dicamba-based products. The same year as the trait approval, the EPA also had 434 dicamba products registered. The first half of the 2010s primarily saw Monsanto petitioning to the USDA to deregulate Dicamba-resistant crops such as

soybeans, cotton, and corn[28]. All petitions filed to the USDA were approved. The approval of these petitions allowed farmers to plant Dicamba-resistant crops on their farms. The first Dicamba-resistant crop planted was Monsanto's Bollgard II XtendFlex Cotton[28]. The spring of 2016 saw more than 100 seed companies sell Dicamba-resistant soybeans for the first time. The issue for this rampant selling of Dicamba-resistant seed was the lack of approval for the promised low-volatility. This was an issue for the agricultural industry because Dicamba has a tendency to become volatile when spraying. This topic will be investigated further in this paper, but for now, Dicamba's volatility is referring to the pesticide's tendency to drift after spraying application and causing off-target injury, which is damage caused to crops that were not the intended target of the spraying application. Following the selling of thousands of Dicamba-resistant seeds without any approved pesticides, the summer of 2016 endured tens of thousands of soybeans acres damaged by off-target drifting from post-emergent Dicamba products. Waves of complaints flooded in from the Midwest and Southeast of the United States. These complaints led to the heightened urgency of obtaining a low-volatile Dicamba-based pesticide. BASF Chemical Company created one called Engenia, which was promised to reduce Dicamba drift by 70%. For this reduction in drift to occur, the spraying protocol had to be closely followed[28,29].

Dicamba Drift

Volatility refers to a liquid herbicide converting to a gas many hours after application and then lifting from the crops and moving many miles in all directions where it recondenses on plants not intended to be covered by the herbicide[30]. This characteristic

of Dicamba is the primary reason why it, along with 2,4-D, has been labeled as the leading pesticide in crop injury by the Association of American Pesticide Control Officers[30]. The effects of Dicamba drift are apparent once it has occurred. Crops not engineered to withstand the effects of Dicamba experience abnormal leaf growth and floral development, reduced quality in the crop, and reduced yields. In addition, injured crops displayed cupped leaves, the stem twists, and leaves experience epinasty, which is the growth of plant cells on the top part of the leaf but not the bottom, leading to drooping of leaves[30,31].

Dicamba drift has caused thousands of complaints over the past five years because of the small fraction of the Dicamba application needed to cause off-target injuries. Approximately 0.005% of the Dicamba application rate kills non-resistant crops[32]. For reference, 1% of glyphosate application rates cause some injuries to off-target crops. In addition, only one gram of Dicamba is needed per hectare, which is less than a hundredth of the usual agricultural application of the pesticide. Crops' heightened sensitivity to Dicamba makes them more susceptible to the active ingredient, which is a major issue for farmers because this is one of the most volatile pesticides used[32,33].

Farmers' mindfulness when spraying Dicamba is crucial because there are multiple ways that can cause Dicamba to become volatile and drift. One of the first things checked when spraying Dicamba is the temperature. It is recommended to take caution in spraying Dicamba when the temperature passes 85°F, which is when the pesticide has a greater tendency to evaporate and drift. Another cause of Dicamba's volatility is its high vapor pressure[32]. This characteristic means Dicamba has an easier time turning into a gas and getting into the air. High vapor pressure compounded with high sensitivity to Dicamba by crops results in the many off-target injuries seen. Lastly, Dicamba is a persistent active

ingredient[32]. This molecule is hard to remove from spraying tanks because it has a longer half-life than other pesticides. Dicamba's half-life is usually one to six weeks but studies have shown to persist even longer[33]. Studies in Florida have seen Dicamba have a half-life of twelve months while studies in Nova Scotia have seen Dicamba have a half-life of thirteen months[33]. If not cleaned thoroughly and properly, Dicamba is mixed with the next pesticide used in the tank. This mixture is sprayed on crops not engineered to endure Dicamba, leading to crop yield reduction and more possibilities for Dicamba drift. Taking these causes of Dicamba drift is essential since over 60 million acres of Dicamba-resistant soybeans were planted in 2019 and 50 million acres were planted in 2018, which is the first year Dicamba-resistant soybeans made up over half the soybeans in the United States[32,33].

The impacts of Dicamba's volatility have led to changes in spraying protocol. One major change is the recommended wind speed when spraying. Before the significant increase of off-target injury complaints in 2016, the recommended wind speed for Dicamba spraying was 15 miles per hour (MPH). Now, the required wind speed for Dicamba spraying is 10 MPH[34]. In addition, farmers are required to spray Dicamba between sunrise and sunset. This is because most and the strongest temperature inversions occur during these hours of the day. New spraying protocol also required farmers to not spray Dicamba if rain is in the forecast for the next 24 hours. This is to prevent Dicamba from drifting onto non-target crops. Dicamba can also not be sprayed in vehicles that are traveling at speeds greater than 15 MPH. When spraying on the edges' of field, spraying protocol requires farmers to not exceed 5 MPH. Speeds exceeding these suggested limits have been shown to increase the likelihood of Dicamba drifting[34]. Lastly, farmers are given spraying protocols to follow a proper order of mixing other pesticides with Dicamba. This mixing

is approved by regulatory companies to ensure that these mixtures do not lead to chemical sprays that have higher volatility[34].

Auxins

As mentioned earlier, the mode of action of a pesticide is the way in which the pesticide initiates a physiological and anatomical change within the plant organism. Dicamba works as an auxin mimicker. Auxin, indole-3-acetic acid (IAA), is one of the two primary growth hormones in plants, the other being Gibberellins. Auxin is known for its role in the regulation of plant growth and development throughout the entire plant[35]. The effects of auxin were first noted by Charles Darwin in 1881. Darwin discovered the importance of auxin through the observances of plants bending towards light sources. After experimenting with his son Francis, Darwin observed that plant growth is controlled by "a matter which transmits its effects from one part of the plant to another." This "matter" Darwin refers to controls key functions in all parts of the plant[36].

Darwin's observations explaining the effects of auxin throughout a plant were discovered in the context of phototropisms. Phototropisms are the orientations of a plant in response to a light source. The plant can either bend towards or away from the light source. In regards to auxins, these hormones cause plants to bend in the direction of the light source[37]. Though Darwin did not know the name or identity of the hormone, the mechanism in which auxins cause plants to move in the direction of light sources has been identified[37]. In the presence of auxins, the cell walls of plant cells become more flexible. Cell walls are composed of a tightly woven matrix of polysaccharides that creates a rigid external for plant cells. For plant cells to elongate, cell walls have to experience turgor pressure from

within the cell for it to expand. To complement the forced cell wall growth by turgor pressure, acidification within the cell wall occurs. This acidification softens the connections between the cross-linked polymers, allowing the cell wall to have more flexibility for expansion[37]. The presence of auxins increases this acidic growth, allowing more plant cells to expand. When a plant senses a light source, it redistributes the auxins to the side of the stem not facing the light. This lateral growth of plants due to auxin movement is referred to as lateral redistribution[37]. This higher concentration of auxins on the darker side of the plant results in greater plant cell growth because more cell walls are being softened. This results in the plant cells on the side not facing the light to grow and be more dominant than those on the side facing the light. As a result, the stem bends in the direction of light because the plant cells on this side are not as large or rigid as those on the side not with the light[37].

Auxins are synthesized in various regions of plants. The primary area is the shoot apical meristem, which are tissue regions in the plant consisting of undifferentiated plant cells. Additional places of auxin synthesis are young leaves and developing fruits and seeds[38]. Analogous to hormones in animals, auxin is synthesized in one part of the plant but travels to all parts of the organism depending on the need of the plant. The mechanism of auxin of biosynthesis is not limited to one pathway. It is postulated that there are multiple biosynthetic pathways that lead to the creation of auxin hormones. The pathway that has been studied the most and viewed as the primary biosynthetic pathway for auxin development is the Tryptophan-Dependent Pathway[38]. This was shown by feeding plants with nutrients containing Tryptophan. Plants that were provided nutrients labeled with Tryptophan followed the pathway that led to the production of IAA. The complete analysis

of this pathway was studied in plants in the *Arabidopsis* genus[38]. This pathway consists of two steps that convert Tryptophan to auxin. This two-step mechanism has been linked with every developmental pathway in plants[38]. The first step of this reaction removes the amino group from Tryptophan. This reaction is catalyzed by the Tryptophan Aminotransferase of Arabidopsis (TAA) family of transaminases. This reaction leads to the formation of the intermediate indole-3-pyruvate (IPA). The IPA then undergoes an oxidation reaction catalyzed by a Flavin-containing monooxygenase of the YUC family. This reaction results in the production of IAA, water, and carbon dioxide. This pathway is highly conserved throughout the plant kingdom[38]. This conservation is due to the developmental and growth emphasis this pathway displays. The understanding of the Tryptophan-Dependent pathway allows molecular processes to be studied by varying auxin concentrations throughout various portions of plants[38].

Auxin's impacts throughout plants are seen in a variety of ways. Auxin is a key regulator in cell division and elongation. The presence of auxin among cells leads to enhance the growth of plant tissue and organs. Auxin's interactions with specific cells lead the cells to particular fates[35]. For example, auxin interacting within cells promote lateral expansion in root while it promotes apical elongation in the shoots of plants. For fruit to grow, auxins are needed to start the development. This process is called parthenocarpy, which is fruit formation without prior fertilization[35]. Auxins induce this process when young, unpollinated ovaries are treated with the growth hormone. Auxins are also present in fruit to prevent fruit senescence, which is biological aging. When injured, auxins induce the formation of xylem and phloem, which make up the vascular tissue of a plant. These cells are formed by auxin because cell differentiation is induced when the wound is

recognized by auxin[35]. Root growth is initiated by auxins. Auxins promote the growth of pre-existing roots while also starting the growth of branching roots from the main portions of the root system[35]. Auxins play a minor role in initiating flowering and the development of the reproductive organs found in flowers. It is evident that auxin plays an important role in promoting growth throughout various regions in a plant, but auxins also have inhibitory roles[35]. Apical dominance is a phenomenon in plants where the central stem is dominant over auxiliary buds coming off the stem. Auxin prevents the growth of these auxiliary buds, ensuring the stem is the dominant part of the plant. Auxin prevents these buds from forming by promoting ethylene synthesis, which inhibits the buds' growth[35].

Mode of Action

Mentioned earlier, Dicamba's mode of action is serving as an auxin mimicker. Dicamba is a member of the Class 4 herbicides where it is in the benzoic acid family. Including the benzoic acid family, Class 4 herbicides also include phenoxyalkanoic acids such as 2,4-D and pyridine-carboxylic acids such as picloram[39]. This class of herbicides is composed of chemical families that interfere with auxin activity. Group 4 has been deemed the Synthetic Auxin class because of its mode of action. The majority of these herbicides in this class control broadleaf plants, which unwanted weeds that are hard to remove from the free areas of fields they overtake[39]. The herbicides in this class share multiple similarities. Just like Dicamba, many of these herbicides exhibit volatility issues due to higher vapor pressures and require lower fraction use rates than herbicides in other classes. The similarity that has classes these pesticides together is the ability to interfere with auxin

activity. The only difference between these herbicides is the active ingredient within the chemical that performs the physiological and anatomical changes[39].

Dicamba, along with the others in Group 4, works as auxin agonist. An agonist, in regards to physiology, is a substance that produces the exact same effects as another physiologically relevant molecule in the body[40]. Dicamba's agonistic effects with auxins cause the plants sprayed with the herbicide to be greatly damaged, potentially leading to plant death. At low concentrations of auxin, which is seen in plants when synthetic auxin herbicides are not sprayed, plants experience growth throughout the entire organism. Plants are able to maintain this low concentration of auxins because plant organisms utilize multiple biosynthetic pathways to inactivate the hormone through degradation and conjugation[40]. When the concentration of auxin increases because of the mimicking effects of herbicides such as Dicamba, plant growth is perturbed and can eventually become lethal[40]. Synthetic auxin herbicides work in various ways. By mimicking auxin, Dicamba induces rapid cell growth throughout the plant, leading to excessive growth rates in the stem, petioles, and leaves of susceptible plants. This rapid growth is the result of Dicamba, and other Class 4 herbicides, affecting cell wall plasticity[40]. This excessive growth is caused by the stimulated activity of the membrane-bound ATPase proton pump in plant cells. The heightened activity of the proton pump in plant cells results in a more acidic environment. This acidifying of the internal environment of plant cells promotes the activity of enzymes whose roles are to loosen polymers in the cell wall, leading to the elongation and growth of plant cells[40]. In addition to changing the pH and rigidity of the cell wall, Dicamba also impacts deoxyribose nucleic acid (DNA), ribonucleic acid (RNA), and protein biosynthesis. The abnormal production of these macromolecules results in

plant cells' uncontrollable cell growth and death because the plant cell cannot maintain homeostasis of the cell's internal environment since more nutrients than available are needed to accommodate the excessive growth. This uncontrolled cell death results in the destruction of vascular tissue throughout the plant[40].

In addition to plants' inability to maintain homeostasis, other mechanisms have been discovered that show how Dicamba leads to plant death. This mechanism shows the deregulation of plant growth, which can be split into three phases. These phases have been studied and a relative timeline after herbicide application has been observed. The first phase is the stimulation phase[40]. This phase occurs within the first hour of spraying. This phase is highlighted by the stimulation of ethylene biosynthesis and symptoms of excessive growth. Ethylene is a key molecule in plants that causes fruit ripening, development of reproductive parts, and flowering promotion[41]. The cell elongation process due to the activation of the proton ATPase mentioned earlier also occurs during this phase. Abscisic acid (ABA) starts to accumulate 5-8 hours after application[40]. ABA's primary functions include stomata closure, bud dormancy promotion, and controls organ size. The second phase of growth deregulation occurs with 24 hours of application. This phase is hallmarked by the inhibition of root growth. The third phase is distinguished by tissue decay and senescence[40]. The biological decay plants endure is due to chloroplast damage and the destruction of membranes and the vascular system. This leads to leaf wilting, necrosis, and plant death. This inhibitory phase applies to all biosynthetic pathways that relate to growth and metabolism. These effects are mainly due to persistently high concentrations of auxin, which is the result of the synthetic herbicides applied to the plants[39].

Chapter 2: Spectroscopy

Spectroscopy is defined as the study of light-matter interactions. To further define, spectroscopy measures the intensity of the sample's response to the light source versus the frequency of the light source. The intensity is the number of transitions between ground and excited states. Frequency is the energy difference between the excited and ground states. The various types of spectroscopy, mainly from the electromagnetic spectrum, have been utilized in multiple science disciplines such as astronomy, biology, chemistry, and physics. Spectroscopy allows both the physical and electronic structures to be analyzed at the atomic level and ranging to the astronomical level. Spectroscopic applications have increased tissue examination, forensic analysis, and pesticide testing.

2A: Electromagnetic Radiation

Light, or electromagnetic radiation, displays a unique characteristic called wave-particle duality. This property means light can act as a wavelength or a particle since it shows characteristics of both simultaneously. Light can only be described as one or the other in one instance. Light is described as a wavelength in most instances[42]. The properties of a wave can be related to electromagnetic radiation through the following equation:

$$c = \lambda\nu$$

This equation shows wavelength (λ) and frequency (ν) are inversely proportional. The constant that relates the two is the speed of light in a vacuum, which is equal to 3 x 10^8

m/s. **Equation 1** is visually represented by the electromagnetic spectrum. This spectrum starts with the lowest wavelength γ -rays which are measured in femtometers and increases in wavelength to radiowaves which are measured in gigameters. The frequency of the electromagnetic radiation increases inversely to wavelength, meaning frequency increases from radiowaves to γ -rays. For the human eye, only a slight fraction of the electromagnetic spectrum can be seen. This range is called the visible spectrum. Light is described as a particle by the following equation[42]:

$$E = h\nu$$

When light is described as a particle, it is called a photon. Photons carry energy proportional to the electromagnetic radiation frequency. A photon has zero mass. The frequency and the energy of the photon are directly proportional and related to Planck's Constant, which is equal to 6.626 x 10^{-34} J*s. Since both of these equations contain frequency, the two formulas can be related using the following equation[42]:

$$E = \frac{hc}{\lambda}$$

With the various parts of the electromagnetic spectrum, there come numerous types of spectroscopy. Each type of spectroscopy has different requirements to make that method viable[43]. A closer look at the requirements of Raman spectroscopy will be discussed later.

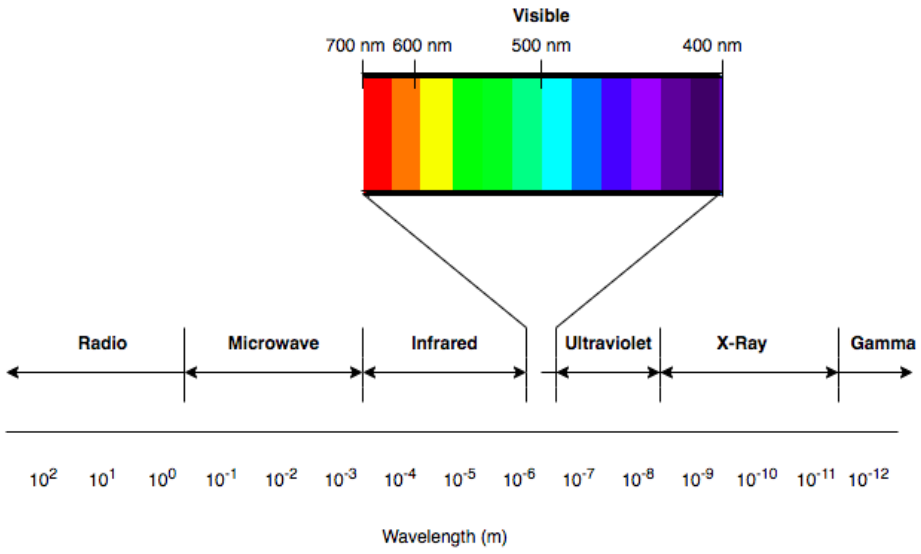

Figure 2.1: The Electromagnetic Spectrum.

2B: Transitions

All matter is always in motion. The type of movement can be different and depends on the matter being studied. A molecule can have four different types of motion: translational, rotational, vibrational, and electronic[44]. Translational motion is the lowest-energy motion of the four. This motion encompasses the entire molecule as the atoms move together throughout the three-dimensional plane[44]. Rotational motion always has an axis of rotation, which usually includes the central atom. The atoms not included by the axis of rotation will spin about the atom on the axis. This motion occurs when electromagnetic radiation is emitted from a microwave source. For the microwave energy to have any effect on the molecule, the molecule must display a permanent dipole moment to provoke the rotational movement[44]. Vibrational motion is higher energy than both translational and rotational motion. Vibrational motion can be described in two ways: stretching and bending. Stretching can further be described as symmetric or

asymmetric. Symmetric stretching occurs when movement on both sides of the atom are in opposite directions but equal magnitude. Asymmetric stretching occurs when there is no uniformity in the movement of the atom. Bending can be described in numerous ways, including rocking, scissoring, wagging, and twisting[44].

Vibrational movements are associated with light sources from the Infrared (IR) spectrum of the electromagnetic spectrum. The last type of motion is electronic motions. These movements are the highest energy of the four motions. Electronic transitions are associated with excitations from the ultraviolet (UV) and the visible portions of the electromagnetic spectrum. Since excitations occur in the visible spectrum, electronic transitions can be seen without any instrumentation when the sample being observed undergoes a color change[44].

2C: Harmonic Oscillator and Anharmonic Approximation

The focus of this experiment is vibrational transitions. Vibrational transitions can be described using the harmonic oscillator the harmonic oscillator is a model that has been used in both classical and quantum mechanics. The harmonic oscillator can be explained by both classical physics and quantum theory. In classical physics, a spring model is considered to describe the harmonic oscillator. This spring is attached to a stationary object with a certain mass, *m*. The force of the spring can be described using Hooke's Law[44]:

$$F = -kx$$

This force described by Hooke's Law is proportional to the displacement of the mass. The spring in this model moves out and instantly returns. The spring, however, does not

return to its initial location. This is shown by the negative sign in Hooke's Law and is called the restoring force. In the equation, *k* is the force constant, which measures the rigidity of the spring[44]. The spring's force can be related to potential energy, assuming $F = \frac{-dV}{dx}$:

$$V = \frac{1}{2}kx^2$$

The equation above represents the energy well shape of the Harmonic Oscillator graph. V represents the harmonic potential, which is the spring infinitely stretching out and infinitely returning in the opposite direction. This equation gives a parabola. For small displacements of the spring, this equation serves as an approximation for the harmonic oscillator of electrons[44].

In addition to the classical physics representation of the Harmonic Oscillator model, there is also an analysis of it using quantum theory. In this representation, two masses are held together by a Hooke's Law spring, meaning the spring requires a force proportional to the distance of displacement to compress or extend the spring. The displacement, x, can be found by comparing the initial location, R, to the equilibrium position, R_e, using the equation $x=R-R_e$. This displacement value can then be substituted into the Hamiltonian function[44]:

$$\hat{H} = \frac{-\hbar}{2\mu}\frac{d^2}{dx^2} + \frac{1}{2}kx^2$$

Energy levels of the harmonic oscillator model are derived from the values of the Hamiltonian's eigenvalues. Eigenvalues are parameters of differential equations that are nonzero under specific conditions[44].

$$E_v = (V + \frac{1}{2})hv_0$$

Where is a quantum number $v_0 = 0,1,2\ldots\infty$

When two masses are attached to both ends of the Hooke spring, the function only has one quantum number. In addition, both masses attached to the spring results in all energy levels are non-degenerate, meaning energy levels have the same energy. These two conditions allow the vibrational quantum number to be calculated using the equation:

$$V_0 = \frac{1}{2\pi}\sqrt{\frac{k}{\mu}}$$

To solve the vibrational quantum number, the reduced mass, μ, and the spring rigidity value, *k*, are needed.

In the harmonic oscillator method, the vibrational energy levels are evenly spaced out. This potential is a parabola. This model is used to represent the vibrational motion of diatomic molecules. The harmonic oscillator is used as an approximation for multiple instances, but it does have some limitations to its approximations. The harmonic oscillator does not account for bond dissociation, meaning the molecule will not break, regardless of how much energy is put in the system[44]. In addition, all transitions occur at the same frequency because of the equal spacing of the vibrational energy levels. This is a key limit to the approximation since multiple energy levels appear during experimentation[44].

The anharmonic approximation is a potential that has deviated from the harmonic oscillator potential. For this approximation, the spacing between energy levels decreases as the vibrational energy level increases[44]. The potential no longer looks like a parabola. The right side of the potential begins to flatten out. Anharmonic perturbations added to the harmonic oscillator describes molecular vibrations better. These deviations from the

harmonic oscillator make the anharmonic approximation a better approximation because it accounts for bond breaking and the anharmonicity of real bonds[44].

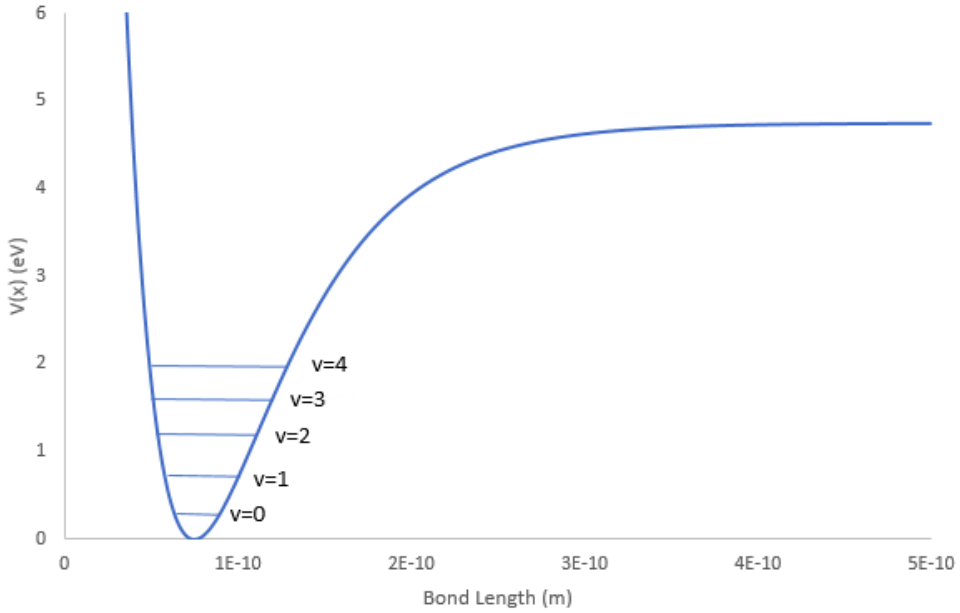

Figure 2.2: Anharmonic Approximation.

Selection Rules

Selection rules determine what transitions are possible. Vibrational transitions in the harmonic oscillator that are allowed are Δ v=+-1. Fundamental vibrational transitions occur when it starts in the ground state. Hotbands are observed when an excited state is further excited. Overtones are observed when Δ v>=-1. They are the result of molecules being anharmonic. Rotational states correspond to a model called a rigid rotor. The rigid rotor model can have transitions Δ J=+-1, where J is the rotational quantum number. There are three branches associated with rotational transitions: Q branch, R branch, and P branch. The Q branch is seen when Δ J=0, meaning that either a vibrational or electronic transition occurred. The R branch is higher energy than that Q branch and is seen when Δ J=+1. In contrast, the P branch is lower energy and occurs when Δ J=-1[44].

2D: Raman Spectroscopy

Raman Spectroscopy is a form of vibrational spectroscopy that analyzes the transitions of electrons, and it is modeled by the harmonic oscillator. Raman Spectroscopy is similar and complementary to Infrared Spectroscopy, another form of vibrational spectroscopy. One major difference between Raman and Infrared spectroscopy is what analysis of the radiation. Infrared spectroscopy, and most other forms of spectroscopy, look at the absorption of radiation whereas Raman spectroscopy looks at the scattering of radiation[44].

In 1928, Sir C.V. Raman and K.S. Krishnan observed light scattering which would later become known as Raman Scattering. Raman and his colleagues were conducting experiments analyzing light scattering in various common liquids. Their light source was the sun, but that alone was deemed too weak to produce observable light scattering. To get a more intense light source, a telescope was used to concentrate the sunlight directly onto the liquid samples, allowing the scatter light's color shift to be seen by. This light scattering was observed to some degree in all liquids studied. Quantitative data was found when Raman measured the exact wavelengths of both the incident light and the scattered light. Raman was awarded the Nobel Prize in Physics for his work in discovering scattering light and discovery of the Raman Effect[45].

For a molecule to be studied using Raman Spectroscopy, the primary requirement is for the molecule to be classified as Raman Active[44]. To be considered Raman Active, the molecule must have a change in polarizability. In contrast, Infrared Spectroscopy focused on molecules' changes in dipole moments. The polarizability of a molecule

measures the tendency of the electron cloud to be affected by an electric field. Distortions in the electron cloud result in the bond length changes[44]. These deviations in bond length lead to affect the polarizability when the molecule vibrates. The change in polarizability of a molecule is the unique characteristic that allows it to be studied using Raman Spectroscopy. When more electrons that surround the nucleus of an atom, the tendency of electron distortion increases causing the polarizability of the atom to increase. This trend can be seen in larger atoms with electrons further from the nucleus. The greater distance increases the likelihood of electron cloud distortion[44].

Light scattering can occur in three ways: Rayleigh scattering, Stokes scattering, and Anti-Stokes scattering. In general, light scattering occurs when a photon collides with a molecule and transfers energy with the atoms of the molecule. This energy transfer between the photon and the molecule excites the molecule to a virtual "excited" state. In Raman spectroscopy, vibrational transitions are seen due to the transmission of energy between the sample and incident light. These vibrational transitions result in vibrational motions that alter the polarizability of atoms within the sample[44].

The scatterings observed in Raman spectroscopy are classified as Raman Scattering, Stokes and Anti-Stokes, and Rayleigh scattering. The main form of scattering seen in nature is Rayleigh scattering. In Rayleigh scattering, the incident light has an equal wavelength as the scattered light. This form of scattering is called an elastic collision because there is no change in the energy or wavelength before or after the light source interacts with the sample[44].

Raman scattering is considered to be inelastic collisions. Inelastic scattering means the interactions between the monochromatic light and the molecule of interest causes the

frequency changes[44]. The inelasticity of the photon is measured before and after the laser light photon has been absorbed and emitted by the sample. The shift of frequency for the reemitted photon can either go up or down depending on the particular molecule being studied. There are two types of Raman scattering observed: Stokes and Anti-Stokes. Stokes scattering is observed when a ground-state electron of the sample matter is excited to a virtual energy state and then comes to rest in an energy state higher than the ground state[44]. The electron does not lower to the ground state because energy from the light source was transferred to the electron. In contrast, Anti-Stokes scattering is seen when an electron begins in an energy state higher than the ground state. The electron is excited to a virtual state and then lower to an energy state lower than the beginning energy level, signifying the sample lost energy to the light source[44]. Raman Spectroscopy is based primarily on inelastic scattering from a single wavelength light source, or monochromatic light. This change of frequency in comparison to the monochromatic light frequency is called the Raman Effect[44].

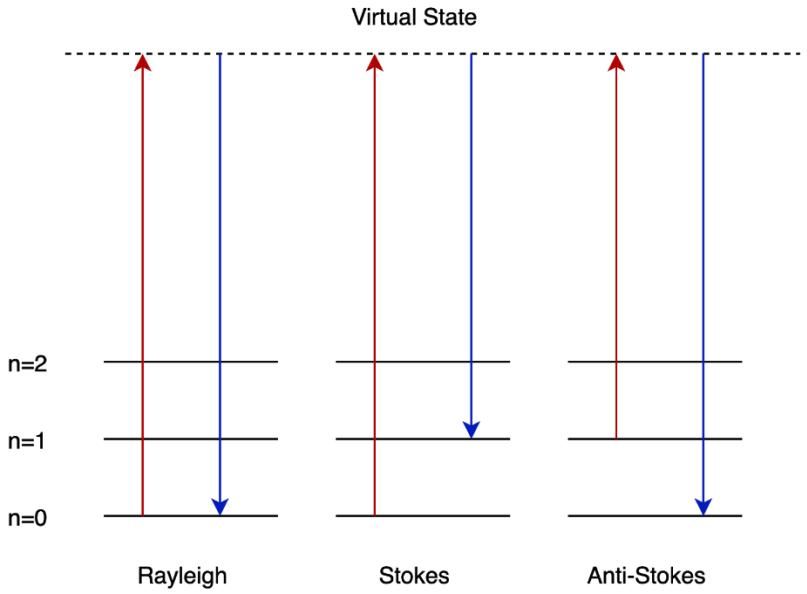

Figure 2.3: Depiction of Scattering.

When analyzing a Raman spectrum, the graph is depicted with intensity on the y-axis and the Raman shift on the x-axis. The intensity is an arbitrary number of a signal is measured at a particular wavelength. The intensity does not have any units. Since the intensity is considered arbitrary, most graphical representations of Raman spectra do not display any values on the y-axis. The x-axis values are measured in wavenumbers. Having wavenumbers on the x-axis shows how IR and Raman spectroscopy are considered complementary. Both have wavenumbers on the x-axis. This similarity is perpetuated by functional groups of molecules sharing showing frequencies in the same regions for both spectra. There is a lower chance of seeing Raman scattering in nature than Rayleigh scattering and IR absorption, and this is why Raman Spectrum has a lower intensity than an IR spectrum[45].

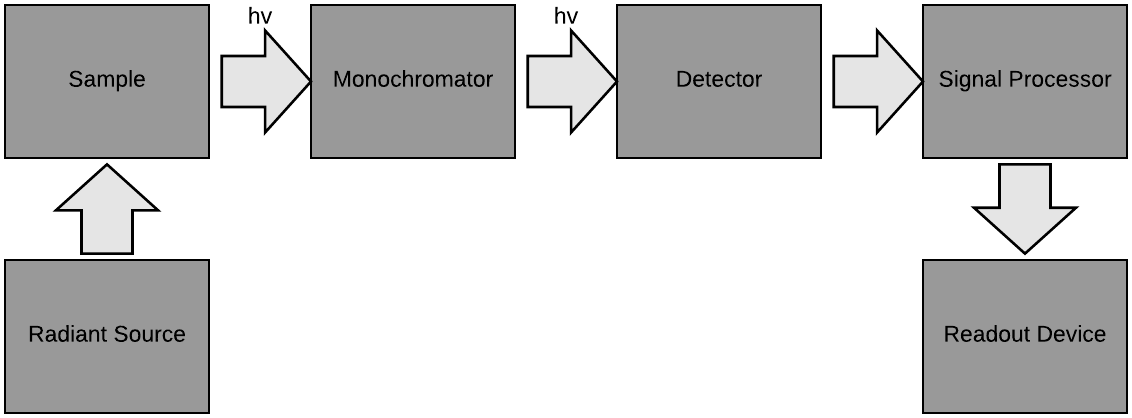

Figure 2.4: Raman spectrometer schematic

In this experiment, a Raman Spectrometer was used. The light source of Raman spectroscopy is usually a laser. The laser used is an intense light source that directly interacts with the sample. The laser is a monochromatic light source, meaning it has the same wavelength throughout the entire laser. Having the same wavelength also means the light source can only be on color. In addition to the laser being monochromatic, the laser needs to display polarizability and be collimating. The laser needs to show polarizability because this characteristic means the wave oscillates in one plane. The laser is desired to be considered collimating because this means the rays from the electromagnetic radiation are parallel. This allows for the laser beam to not spread much over any reasonable distance. The laser causes excitation of the sample matter. The energy generated to cause this excitation is caused by a population inversion. This phenomenon occurs when more electrons in the sample excited stated than the lower energy ground state.

Chapter 3: Theory

Quantum chemical calculations have developed since the advent of reliable computer software in the 1940s, allowing the existence of a viable alternative to conducting chemical calculations without experimental procedures. These calculations fall into a field of chemistry referred to as Theoretical Chemistry. This sector of chemistry is large in the sense that new programs and approximation provide chemists with the opportunities to study chemistry in ways not possible before the creation of computers. Molecules that chemists never thought could be studied now can be observed in the theoretical realm of chemistry, allowing these molecules' vibrational modes, molecular structure, lowest-energy conformation and much more to be studied with accuracy. The advancements of computers have provided chemists with the means to study all aspects of a chemical reaction and also compare the experimental results with data collected by the computer. Technological advancements made computational chemistry software to be commonplace in many laboratories. This is due to the majority of these programs not needing significant specialized training.

3A: Potential Energy Surfaces

General chemistry courses have taught the essentials of understanding the equilibrium of a chemical reaction. A chemical formula depicts a chemical reaction as being comprised of only reactants that turn into products. The in-between steps represented

by one arrow are not as insignificant as a chemical formula may make them seem. These in-between structures, or transition-states, can provide pertinent information about the entire chemical reaction. A transition-state is an activated form of a molecule in which the molecule has undergone a partial chemical reaction; the highest point on the reaction coordinate[46]. A reaction coordinate is a diagram that shows the energy fluctuations of a chemical reaction. The peak of the reaction coordinate is the transition-state complex whereas the minima for the diagram are the reactants and products. Reactants and products are minima for the energy diagram because these two instances of the reaction represent the most stable molecules throughout the chemical reaction. This heightened stability results in reactants and products being the lowest-energy states. Though the beginning and the endpoints of a chemical reaction are low-energy states, the chemical reaction does not maintain this level of low energy throughout[46]. As previously noted, the transition-state complex of a chemical reaction is referred to as the energy maxima of the reaction. The chemical reaction rises in energy as it changes from reactants to transition-state and then decreases in energy as the product is formed.

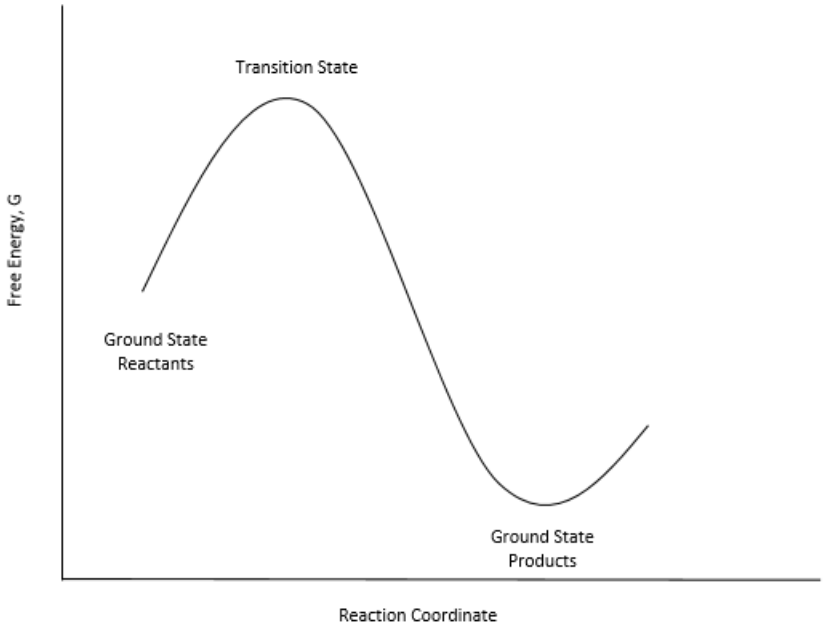

Figure 3.1: Reaction coordinate displaying reactants, transition state complex, and products with relative energies.

The reactants, products, and transition states of a chemical reaction are all stationary points. A chemical reaction is fluent in the sense that there is never a point where one instance of the chemical reaction is solely fixated on one molecular conformation. The perpetual changes that occur within a chemical reaction make the experimental investigation for these intermediary steps. As mentioned earlier, these steps between reactants and product formation could not be studied until the advent of reliable computer programs. Theoretical calculations provide the means to study reaction transition states, which cannot be observed, and highly reactive molecules, which may be difficult to synthesize properly in a laboratory. This allows all potential conformations of the molecule to be studied during a chemical reaction. For these theoretical calculations, quantum chemistry software has been created to make the necessary approximations needed to solve the Schrödinger equation. The Schrödinger equation is a linear partial differential equation that is used to describe wave and state functions of quantum-mechanical systems[46]. The

issue for the Schrödinger equation is that it cannot be solved for a multi-electron system, meaning the only possible system that can be solved is a hydrogen atom or other one-electron systems. For this reason, many approximations have to be made in theoretical calculations for the Schrödinger equation to be solved for the molecule or system being studied. When solved, the Schrödinger equation provides the lowest possible energy conformation of the molecule that can be theoretically determined[46].

3B: Hartree-Fock Molecular Orbital Theory

As stated previously, it is impossible to solve the Schrödinger equation for any system other than a hydrogen atom. Despite this limitation, approximations can be made, leading to an estimated value for the Schrödinger equation, which is shown below.

$$\hat{H}\Psi = E\Psi$$

E represents the total amount of energy. Ψ specifies the n-electron wave function, which depends on both the identities and positions of the nuclei and the number of electrons. $\hat{H}$ is the Hamiltonian, which is the total kinetic and potential energies of the particles[44].

There are three approximations that have to be made for the Schrödinger equation to solve multinuclear and multi-electrons systems. The first is the Born-Oppenheimer approximation. This approximation makes use of the fact that nuclei move much slower than electrons. As a result, it can be assumed that the nuclei are stationary in regard to the electrons. This assumption leads to the electronic Schrödinger equation[44].

$$\hat{H}^{el}\Psi^{el} = E^{el}\Psi^{el}$$

Even though the Born-Oppenheimer approximation is made, the electronic Schrödinger is still insolvable for every case other than one-electron systems. For this reason, more approximations must be made. The next approximation made is the Hartree-Fock approximation, which assumes all electrons in the system more independently of one another[44]. This is done by assuming each electron is contained to functions called spin-orbitals. Each electron feels an average electric field of all other electrons. The final assumption made is that the wave function is antisymmetric in regard to electron coordination interchange[44]. To ensure this happens, the wave function is written as a single determinant called the Slater Determinant. For the wave function to be antisymmetric, the Slate Determinant must equal zero[44]. This is achieved by the assumption from the Hartree-Fock approximation that electrons must be paired. A spin-orbital is composed of only two spin functions, α and β, giving the notion that the maximum number of electrons in a spin-orbital is two. To satisfy the Pauli Exclusion Principle, the electrons paired in the spin-orbitals must not be the same orientation, preventing two electrons from the same quantum state being in the same orbital[44]. When the spin functions of the determinant are multiplied, the different spin coordination leads to the determination equaling zero and inevitably leading to the wave function being antisymmetric. The issue with this assumption that electrons are paired is that there any many instances where electrons are not paired.

The self-consistent field (SCF) refers to molecular orbitals that lead to the lowest-energy structure to be obtained by computational calculations using the Hartree-Fock

method. The data collected by this method and the Hartree-Fock approximation results in a set of differential equations that are called Hartree-Fock equations. Each of these equations represents the coordination of an individual electron in the system being studied[44]. It is challenging to solve the Schrödinger equation for multi-electron systems, even with multiple approximations. This is why each electron in the system has its own differential equation. It is assumed that to the sum of multiple differential equations each representing one electron can provide an accurate approximation of the multi-electron molecule's wave function. The introduction of more approximations allows for the Hartree-Fock equations to be turned into sets of algebraic equations that can be solved more easily. This concept of converting differential equations into solvable differential equations is called the linear combination of atomic orbitals (LCAO) approximation[44].

The Hartree-Fock method was one of the first computational chemistry theories established, which was soon after the discovery of the Schrödinger equation. This version of the computational theory has experienced significant use since its creation. Despite this frequent use, the Hartree-Fock method does have some limitations that have led to the creation of new methods and approximations to be produced. The main source of the Hartree-Fock method's limitations results from the extent of electron correlation[44]. The Hartree-Fock approximation replaces instantaneous interactions between electrons with an interaction between electrons and a charged cloud composed of all other electrons[44]. The assumption that all other electrons result in the introduction of rigidity throughout the electron cloud. If each electron was assumed to be an individual entity, there would be more flexibility for electrons to move among one another[44]. Since electrons are not considered as individuals, electrons are not able to maneuver one another as well since the

remaining electrons are considered one charged cloud. This reduction in flexibility leads to an increase in repulsion energy among electrons, which eventually becomes too large to represent true answers to the Schrödinger equation. The main deviation from the Schrödinger equation that causes the Hartree-Fock method to have a limiting factor is called correlation energy[44]. This term is referred to as correlation energy because this energy accounts for electrons adjusting or correlating to the motion of surrounding electrons[44]. The Hartree-Fock approximation's restriction on electrons' ability to adjust freely to surrounding electrons decreases electrons' capabilities to properly correlate to their surroundings. Limiting Hartree-Fock models can be shown by understanding issues that arise with reaction energies, equilibrium geometries, vibrational frequencies, and dipole moments[44].

3C: Density Functional Theory

Two very different approaches that have allowed chemists to move past the Hartree-Fock method. The first is the Roothaan-Hall method, which increases the flexibility of the wave functions produced by the Hartree-Fock method by combining wave functions the Hartree-Fock functions with wave functions of varying excited states[44]. The second approach, and one that will be discussed in more detail, has allowed an explicit Hamiltonian value to be introduced to account for the interdependence of electron movement[44]. This approach is called the Density Functional Theory (DFT). DFT is another version of computational quantum mechanical modeling that is used to study physics, chemistry, and other science-based disciplines. DFT was created to move past the Hartree-Fock method so that the limitations of Hartree-Fock could be avoided[44]. DFT is based on

the exact solution for an idealized many-electron problem, more specifically working under the notion of an electron density with a uniform density. Part of the answer to this problem is that all associations with exchange and correlation contributions are removed and incorporated into an SCF formalism that is greater similar to Hartree-Fock formalisms[44]. Since the exchange and correlation contributions are now originating from an idealized problem, DFT is not limited to an exact solution of the Schrödinger equation. The reason that DFT is not limited to an exact answer to the Schrödinger equation is that it brings in external data, which is the needed component to solve the idealized problem[44]. The incorporation of external data is one key factor that allows DFT to surpass Hartree-Fock. For the energy of the total system to be solved for, six components are needed.

$$E^{DFT} = E_T + E_V + E_J + E_{NN} + E_{XC} + E_{corr}$$

These six energy components are E_T, the kinetic energy of the electrons, E_V, the nuclear-electron repulsion energies, E_J, the electron-electron Coulomb repulsion energies, E_{NN}, the nuclear-nuclear repulsion energies, E_{XC}, the non-classical electron-electron exchange energies, and E_{corr}, the correlated movement energies of electrons with different spins[44]. This varies from the Hartree-Fock method because DFT accounts for the electron-electron exchange energies whereas Hartree-Fock does not. Essentially, DFT was created to predict how electrons affect one another in an idealized problem. DFT accounts for more individual characteristics of electrons, making calculations more accurate. In addition to accounting for exchange energies and correlation effects, DFT also presents an opportunity to conduct computational calculations at a lower price than the Hartree-Fock method and

any descendants of Hartree-Fock. An issue that arises for DFT is that this form of computational theory has difficulty accounting for and describing intermolecular interactions such as van der Waals forces, transition states, and charge-transfer excitations[44].

The creation of computational approaches such as DFT shows that theoretical chemistry is moving in a direction to find more accurate and less limited forms of quantum mechanical computations. Though Hartree-Fock was the first form of quantum mechanical computations, it has some significant limitations that cause deviations from the Schrödinger equations that are far too large. DFT, though not perfect either, displays the progress being made in the field of computational chemistry to accommodate for limitations that have arisen from the Hartree-Fock method[44].

3D: Optimization and Frequencies

Theoretical computations were done to compare to collected experimental data. The structures that were studied were run in a Gaussian program where the lowest-energy structure was optimized before calculations were run. Next, these structures were analyzed to find simulated frequencies of vibrations that would have been observed using experimental Raman spectroscopy. The optimized structure corresponds to the minima of the graph shown in **Figure 3.1**. Though the optimized geometry is correlated to the reaction coordinate minima, the structure does not always have the lowest energy. This is allowed for geometry calculations because the optimized geometry still has lower energy than the starting structure's geometry. To optimize the geometry of a molecule, the first derivative of each potential coordinate on the reaction coordinate diagram. The data from these

derivatives are used to get an idea of the most optimized geometry. The energies of guessed structures are determined. For a guessed structure to be deemed correct, the potential energy of the reaction coordinate must equal zero[44].

3E: Method and Basis Set

B3LYP

Many methods arose when the DFT method grew in prominence. One of these new methods included B3LYP. B3LYP stands for Becke, 3-parameter, Lee-Yang-Parr. It was first developed to analyze circular dichroism and vibrational absorption. The emergence of B3LYP was greatly welcomed because it has shown accurate results but does not cost as much as other computational options. One of the primary subsets of molecules studied by B3LYP is organic gases. This method is a hybrid functional, meaning that exchange-correlation energy from DFT is combined with exact exchange energy from Hartree-Fock. This incorporation of DFT and Hartree-Fock data allows for more accurate calculations. The idea of hybrid functional is not just limited to B3LYP. There are multiple hybrid functionals used in various computations calculations, the difference between the hybrid functionals is the mixing parameters of the varying options. For B3LYP, the exchange energy is found using three mixing parameter[44]:

$$E_{XC} = 0.2 * E_X(HF) + 0.8 * E_X(LSDA) + 0.72 * DE_X(B88) + 0.1 * E_C(LYP) + 0.19 * E_C(VWN)$$

In this equation, HF stands for Hartree-Fock. LSDA stands for Local Spin Density Approximation. D88 is a gradient correction. LYP is another gradient correction factor determined by Lee, Yang, and Parr. VWN is a correlation functional discovered by Vosko, Wilk, and Nusair. The scaling factors for this hybrid functional method were derived by fitting the data to thermochemical data[44].

6-311++G(*d*,*p*)

6-311++G(*d*,*p*) is a split valence basis set. This means that the inner set of electrons is represented by one set of functions while the outer electrons are represented by another set of functions. This basis set is primarily used for smaller organic molecules. The benefit of 6-311++G(*d*,*p*) is that it is not a costly computation. 6-311G(*d*,*p*) adds polarization functions to hydrogens of the 6-311G* basis set. The ++ portion of the basis set accounts for hydrogen's s-type diffuse functions. Diffuse functions are shallow Gaussian functions that represent the furthest part of an atomic orbital from the nuclei. These functions assist in calculations with larger and more electronegative atoms. The d and p functions account for larger atoms in the molecule[44].

Chapter 4: Experimental and Theoretical Results and Discussion

The purpose of this experiment was to find an agreement between experimental and simulated Raman spectra of Dicamba. In addition to studying Dicamba as an individual molecule, it was further studied by creating various simulated environments. These included Dicamba as a dimer and Dicamba with varying amounts of water molecules in conjunction with varying functional groups of the molecule. Once computational calculations were completed, the Raman spectra were further analyzed by studying the shift in individual modes in the various simulations constructed. Experimental results were collected by using a Raman spectrometer. Theoretical results were calculated using a Gaussin16 program. The end goal of this experiment was to compare experimental and theoretical for all environments created in the Gaussian16 program. This could not be completed, however, due to the interruption in the academic year due to COVID-19. Though the final results could not be completed for this document, comparisons were made between experimental and theoretical data when possible. In addition, theoretical results were compared among one another when applicable.

4A: Experimental Results

To obtain experimental results, a Raman spectrometer was used. The spectrum was collected using the second harmonic (532) output from a YAG:Nd laser. The Dicamba sample studied was a white powder. The experimental spectrum is shown in **Figure 4.1**.

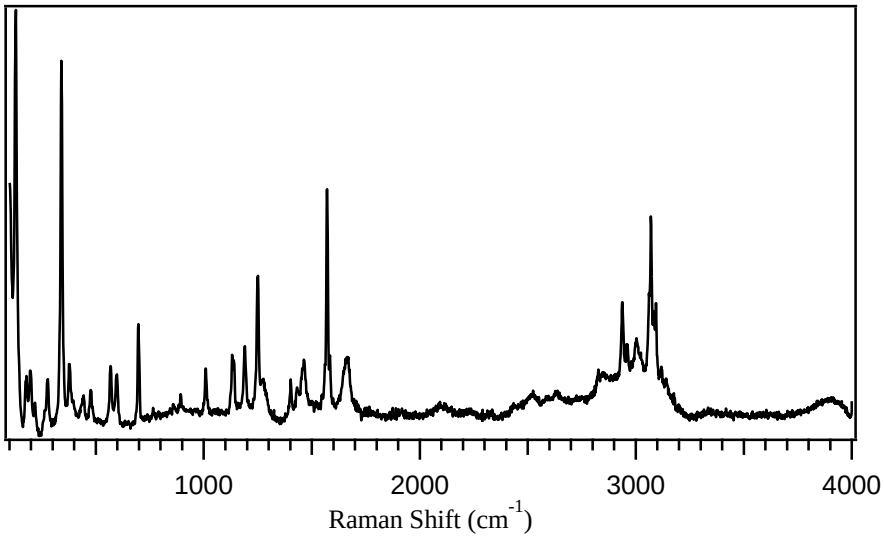

Figure 4.1: Experimental Raman spectrum of Dicamba.

The figure above shows an experimental Raman spectrum of Dicamba. In this figure, the vibrational modes of interests are the peak at 1800 cm^{-1} and the 3500 to 4000 cm^{-1} range. The peak at 1800 cm^{-1} corresponds to the stretching of the carbonyl on the carboxylic acid functional group. The the 3500 to 4000 cm^{-1} range corresponds stretching of the hydroxyl functional group. In simulated envrionments seen later, sharp peaks corresponding to the hydroxyle stretch will be in the place of the broad, flatten portion of the spectrum seen above. This is most likely due to the fact that all simulated instances contain at most two Dicamba molecules interacting with one another whereas the crystalline powder studied contains far more interactions among the Dicamba molecules within the crystalline structure. The reason in which multiple interactions result in a broaden portion of a spectrum is that each interaction adds a new peak to the area of interest. As more peaks are added to this region, overlap begins to occur. This overlap eventually results in the flattening of the individual sharp peaks. As more peaks are added, the region morphs from

multiple sharps peaks close together to the flatten, broad region seen in the 3500 to 4000 cm^{-1} range on **Figure 4.1**. These regions of the spectrum are of great interest because water molecules and other Dicamba molecules interact with these functional groups of Dicamba.

Five different Dicamba samples were studied using the Raman spectrometer. **Figure 4.1** represents the best data collected of the five samples studied. The reason for this selection is that this spectrum has the least amount of background noise compared to the other four spectra taken. This spectrum is the only experimental spectrum that will be provided in this report. This is due to the interruption of the academic calendar due to COVID-19. The goal of this thesis coming in was to study Dicamba as a crystalline powder, which is shown in **Figure 4.1**. In addition to this, the plan was to study Dicamba while dissolved in water. This portion of the experiment did not occur before the closing of academic buildings, so the spectra were not able to be obtained. As a result, only simulated spectra containing water molecules will be compared since there is no experimental data to be collected. The data from **Figure 4.1** will be compared to specific simulated spectra shown later in the Results section.

4B: Theoretical Results

The purpose of using Gaussian16 was to create theoretical Raman spectra for varying combinations of Dicamba and water molecules. Though these spectra are optimized and do not display how environmental factors would affect experimental data, these spectra provide means of comparison for experimental data collected. The comparisons made in this report are done to see if there is agreement between simulated and experimental spectra and to see if there are shifts in vibrational modes of specific

functional groups. The multiple combinations of Dicamba and water molecules will be presented as individual spectra. After all spectra have been reported, comparison between spectra and vibrational modes will be made.

All simulated spectra were constructed the same way in which the experimental spectrum was made. The x-axis represents the Raman shifts which are in wavenumbers. The y-axis represents the Raman intensity. The only difference between experimental and theoretical spectra is that theoretical spectra require a scaling factor. This scaling factor is applied to the x-axis values to account for anharmonicity. The scaling factor applied to the wavenumbers of each theoretical spectra is 0.98.

The theory for all theoretical spectra remained the same. The method for each was B3LYP. The basis set was 6-311++G(*d*,*p*).

Simulated Dicamba Spectra: One Dicamba and Dimer Systems

The first simulated calculation run was of just one Dicamba molecule. This spectrum will be compared to the experimental data in **Figure 4.1** later in the Results section. **Figure 4.2** represents the simulated Raman spectrum for one Dicamba molecule.

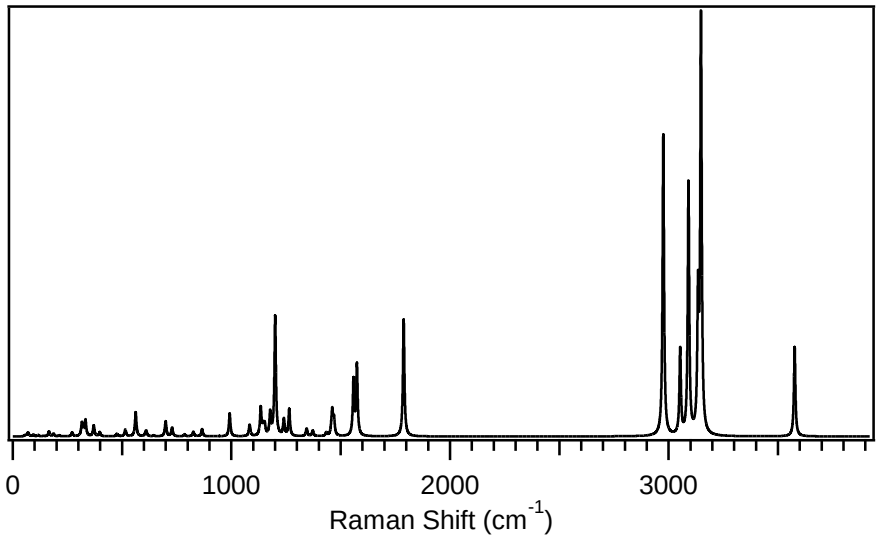

Figure 4.2: Simulated Raman spectrum of Dicamba.

The vibrational modes of most interests shown in **Figure 4.2** are the carbonyl stretch at 1824.53 cm^{-1} and the O-H stretch at 3649.33 cm^{-1}. These vibrational attract more interest than others due to the impact the introduction of additional molcules have on the Raman spectrum. The sharp peaks around 3000 cm^{-1} represent variations of symmetric and asymmetric C-H stretching throughout the molecule. Though these peaks are the most intense, C-H stretching is not impacted as much by the addition of Dicamba and water molecules.

A general trend that has been observed when additional molecules are added is that the intensity of peaks in the region ranging from approximately 1000 cm^{-1} to 2000 cm^{-1} decreases. Vibrational modes within this region include benzene bending and stretching and carbonyl stretching. This region of the Raman spectrum can be seen in **Figure 4.3**.

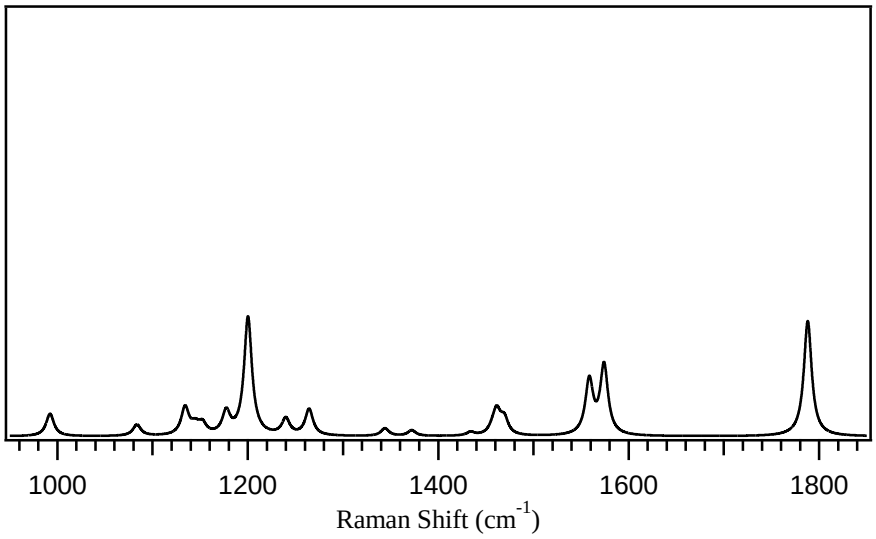

Figure 4.3: Dicamba simulated Raman spectrum focused on the 1000 cm^{-1} to 2000 cm^{-1} range.

Upon completion of the analysis regarding the individual diacmba molecule, the next simulated environment studied was a Dicamba dimer system. The purpose of studying this system was to analyze the effects interactions between Dicamba molecules display with the hopes of mimicking the actual effects interactions within a crystalline structure of Dicamba would have on a Raman spectrum. Two different Dicamba dimer systems were analyzed. The first consisted of two Dicamba molecules constructed using the GaussView 6 program. The geometry of this system was founding by optimzing the structures first. Using optimization as the first step of the process finds the lowest point on the potential energy surface diagram, which was mentioned in Chapter 3. Once the optimized structure was obtained, a second calculation was run with freq=raman in the comand line. This command is what initiates the calculations necessary to determine the Raman spectrum for the given system. The first Dicamba dimer system Raman spectrum can be seen in **Figure 4.4**.

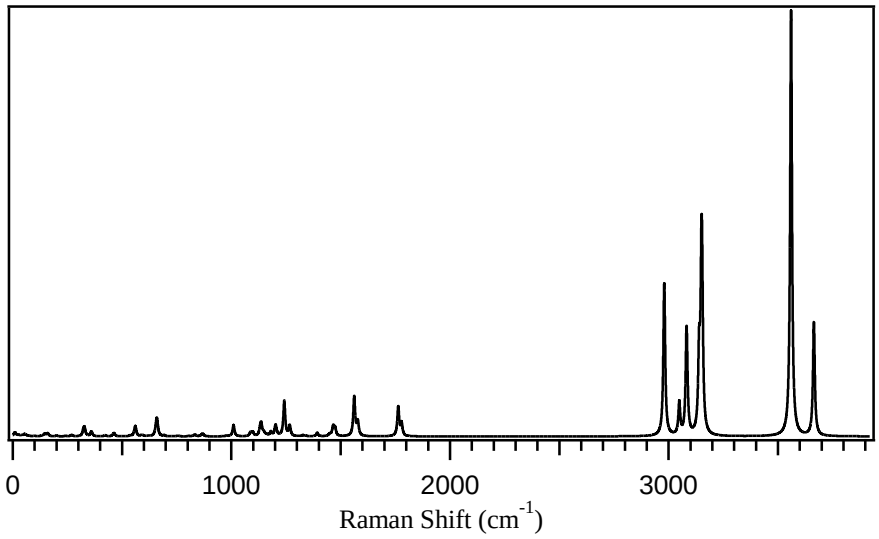

Figure 4.4: Optimized Dicamba dimer simulated Raman Spectrum.

The second Dicamba dimer system was not constructed using GaussView 6 program. This system already constructed using a crystal structure database. The difference between the dimer system retrieved from the database and the optimized dimer system is that the file from the crystal structure database is oriented to match how Dicamba molecules would be oriented within a crystalline structure. The file of the Dicamba dimer was used to create a theoretical Raman spectrum for the purposes of comparing with experimental spectra to see if there is any agreement between the spectra.

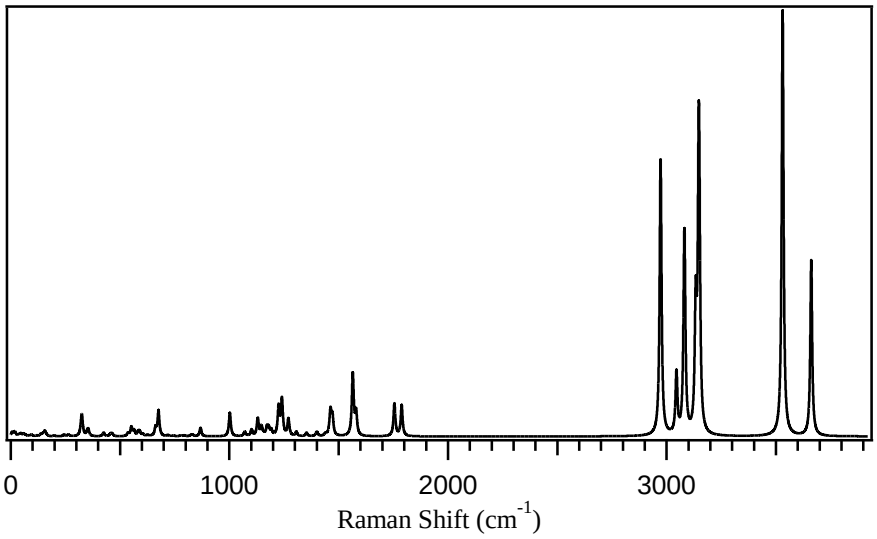

Figure 4.5: Simulated Raman spectrum of Dicamba dimer system from crystal structure database.

At first glance, the two spectra of the Dicamba dimer systems display similar vibrational modes, but after a closer analysis, there are variations between the two spectra. **Figure 4.6** displays the two spectra beside one another for a closer comparison with the optimized dimer spectrum on top and the crystal structure database spectrum on the bottom. The main difference that is noticeable between the two spectra in **Figure 4.6** is the intensity of peaks in the crystal structure database spectrum. Peaks with greater intensity include those representing various vibrational modes for C-H stretching ranging from 2900 to 3200 cm^{-1}. In addition, the O-H stretch at 3736.16 cm^{-1} displays a sharper peak on the crystal structure spectrum than the optimized dimer spectrum, which shows O-H peaks at 3632.61 cm^{-1} and 3739.17 cm^{-1}. The crystal structure database dimer also displays another O-H peak at 3602.30 cm^{-1}. These systems display two O-H stretch vibratioanl modes because there are two of these vibrational modes present. The crystal structure database dimer system has two O-H peaks with vibrational modes at lower energies than those of the optimized dimer. This can be accounted to the fact that the crystal structure database system has a more

optimzed geometry than the GaussView dimer, which allows for more stabilizing interactions and lead to lower energy vibrational modes. Both spectra also display two carbonyl stretches. The optimized dimer structure has these vibrational modes at 1799.05 cm^{-1} and 1814.73 cm^{-1}. The crystal structure database dimer displays these peaks at 1790.58 cm^{-1} and 1824.53 cm^{-1}. Though both carbonyl vibrational modes for the crystal structure dimer are not at lower energies compared to both peaks of the optimized dimer structure, the peak at 1824.53 cm^{-1} for the crystal structure dimer is the same energy as the carbonyl stretch for the one Dicamba system, which would be expected since this dimer system is more optimized. One additional difference is the increase in amount of peaks in the 1200 to 1850 cm^{-1} range. A more foucused look at this region can be seen in **Figure 4.7**.

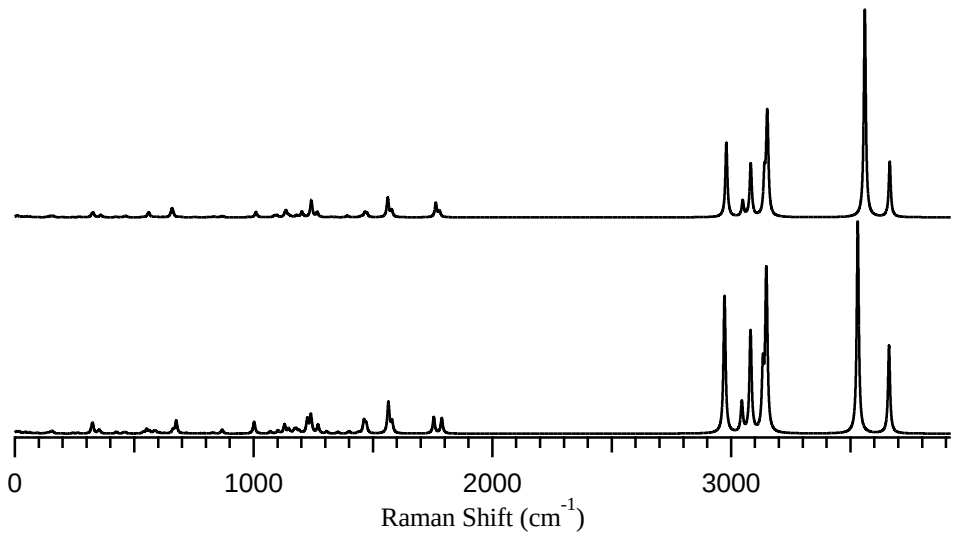

Figure 4.6: Comparison between two Raman spectra of simulated Dicamba dimer systems. The top spectrum is the optimized dimer spectrum. The bottom is the crystal structure database spectrum.

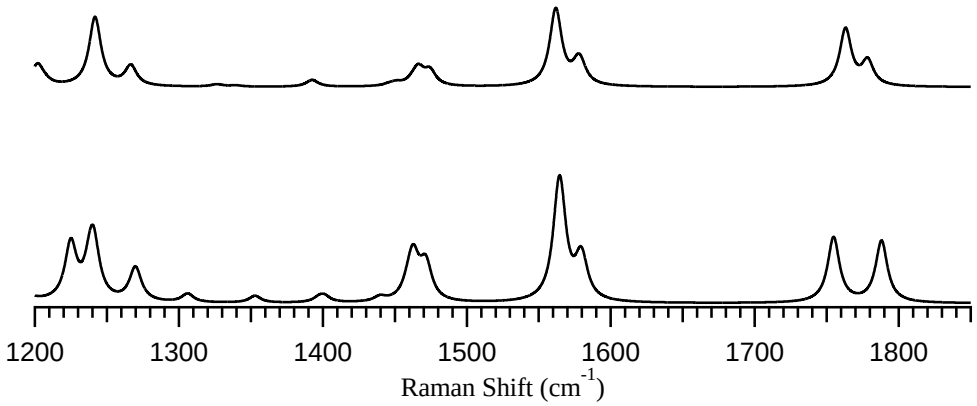

Figure 4.7: Comparison of Dicamba dimer systems from 1200 to 1850 cm^{-1}.

The increase in peaks seen in the 1200 to 1850 cm^{-1} region of the crystal structure spectrum is most likely due to the increase in interactions between the Dicamba molecules in the crystal structure system because of the more optimized positioning between the two Dicamba molecules than in the optimized dimer system.

In addition to comparing the dimer systems between one another, comparisons between the individual Dicamba molcule, the dimer systems, and the experimental spectrum were made. **Figure 4.8** shows the similarities and differences between the theoretical Raman spectrum of one Dicamba molecule and the experimental data collected of the Dicamba powder studied. Though there is some background noise still present in the experimental results, some comparisons can still be made. Some of the most apparent similarities are the peaks centered at 3000 cm^{-1}. As mentioned previosuly, these peaks correspond to C-H stretching throughout the molecule. Another similarity seen between the two spectra is the benzene bending peak, which is at approxamately 1250 cm^{-1} for the experimental spectrum and 1224.71 cm^{-1} for the theoretical spectrum. One of the more

distinct differences between the two spectra is the difference of postion of the carbonyl stretching peak. For the theoretical spectrum, the carbonyl stretching peak is at 1824.53 cm^{-1}. The same peak on the experimental data spectrum is at approximately 1650 cm^{-1}. This shift in energy is most likely due to stabilizing effects of the crystalline strucutre. The experimental sample contains multiple dicamba molecules which hydrogen bond with one another. These stabilizing interactions result in a decrease in this peak energy, which is deemed a red shift. The last main differnce seen between these two spectra is the one singular peak representing O-H stretching in the theoretical spectrum and the broad, flat region in the experimental spectrum. As mentioned previsouly as well, the appearance of the O-H stretching peak is sharp and distinct because there are no other peaks in that region to overlap with this peak. The addition of numerous O-H stretching peaks due to the crystalline structure in the experimental results in significant overlap of the O-H peaks from all the Dicamba molecules in the crystalline structure. This inevitably leads to the broad, flat region of the experimental spectrum.

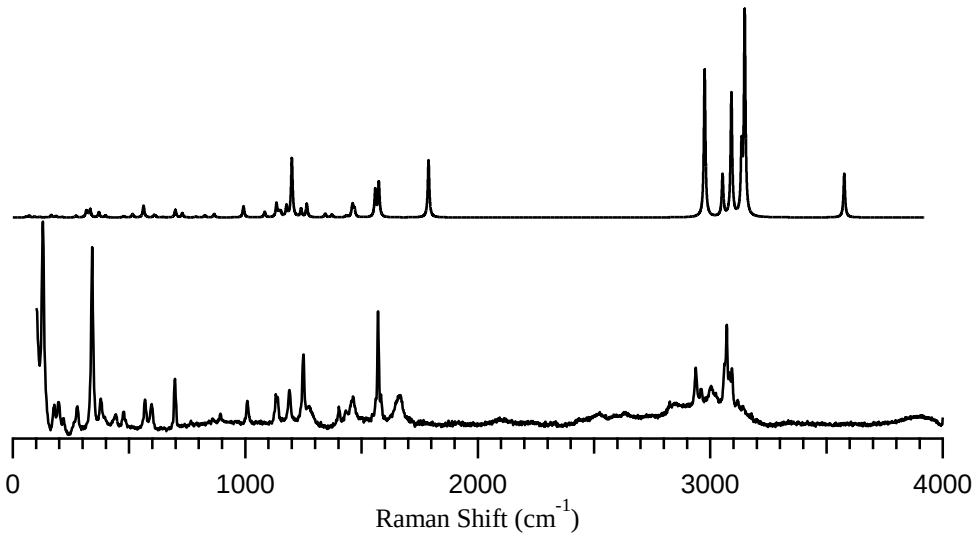

Figure 4.8: Theoretical Raman spectrum of one Dicamba molecule and experimental spectrum of Dicamba sample.

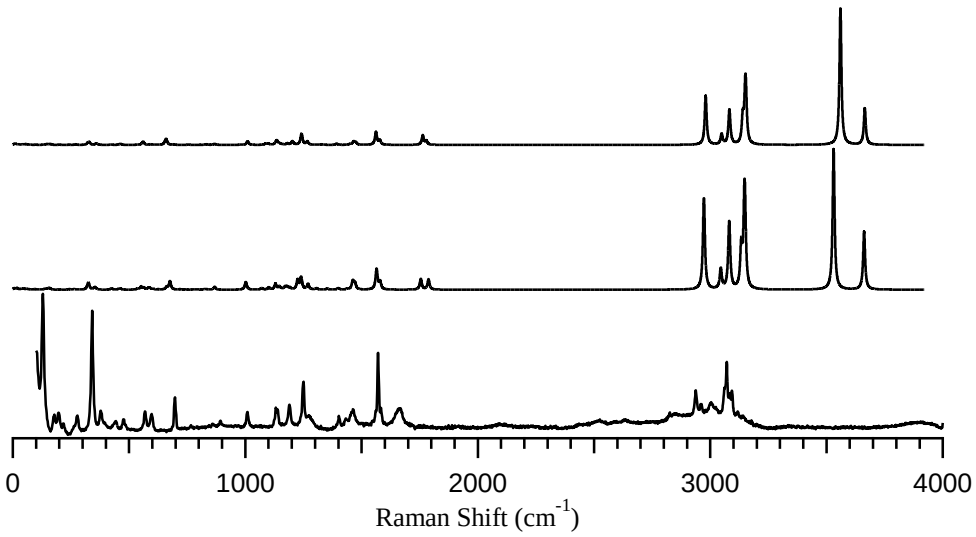

Figure 4.9: Comparison between theoretical dimer systems and experimental data.

In addition to comparing one theoretical Dicamba molecule to experimental data, the Dicamba dimer systems were compared to the experimental spectrum. The same similarities and differences discussed about the dimer systems remain the same when comparing these spectra with the experimental spectrum. **Figure 4.9** shows the dimer systems being compared with the experimental spectrum where the optimized dimer spectrum is on top, the crystal structure database spectrum is in the middle, and the experimental spectrum is on the bottom. One of the main distinctions is again the broad, flat region of the experimental region and the two peaks within the region on the dimer system spectra. This difference has the same reasoning as the comparison of one Dicamba molecule system and the experimental results. Another difference to note is the variation in the carbonyl stretch between the dimer systems and the experimental data. The crystal structure dimer system displays a carbonyl stretch peak at 1790.58 cm^{-1}. The optimized dimer system displays a carbonyl stretch peak at 1799.05 cm^{-1}. The experimental peak for a carbonyl stretch is approximately at 1650 cm^{-1}. The speculated reason the experimental

carbonyl stretch has shifted lower in energy is the same as the comparison between the one Dicamba molecule and the experimental data. There are far more stabilizing forces in a crystalline structure of Dicamba than a dimer system, which is why the carbonyl stretch peak is seen at a lower energy for the experimental data.

The last comparison to be made between systems containing only Dicamba molecules is one between the dimer systems and the individual Dicamba molecule. This comparison can be seen in **Figure 4.10**. One of the most obvious differences is the addition of a second peak for the dimer systems at approximately 3700 cm^{-1}. This second peak corresponds to O-H stretching. This peak addition to the dimer spectra is logical because the addition of a second molecule creates another opportunity for O-H stretching. One other distinct difference among the three spectra is the intensity of peaks in the 1000-2000 cm^{-1} region. As seen in **Figure 4.10**, the peak intensity of this region is far greater for the one Dicamba spectrum that the dimer system spectra. This can be attributed to the functional groups of the one Dicamba system being more distinct since there is not another molecule with the same functional groups. Another general trend that can be observed is that the positions of the peaks do not change drastically throughout the three spectra. In other words, the vibrational modes are not greatly shifted after an additional Dicamba molecule has been added to the system.

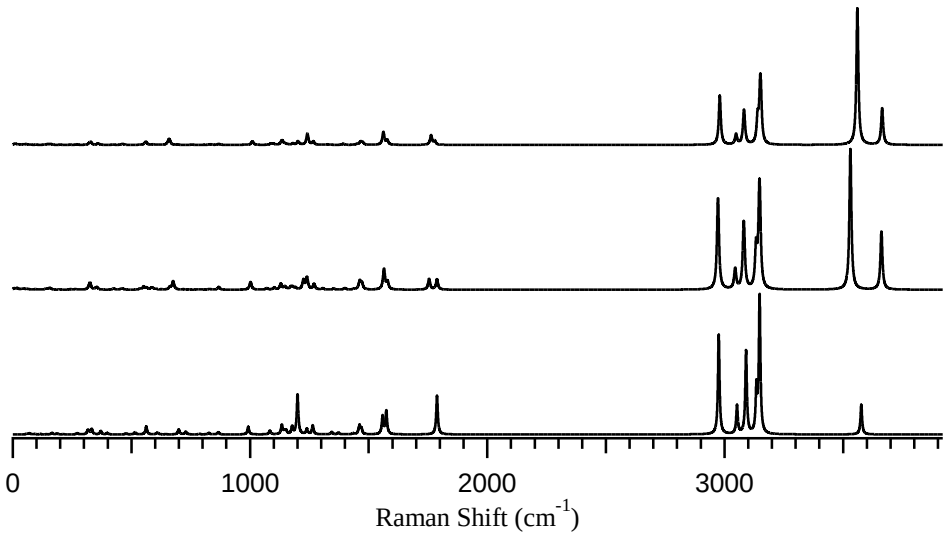

Figure 4.10: Comparison of theoretical Dicamba systems with the optimized dimer system on the top, the crystal structure database spectrum in the middle, and the one Dicamba spectrum on the bottom.

Simulated Dicamba Spectra: One Water Molecule

The purpose of second portion of this study was to see how various combinations of water molecules in different amounts and positions would impact the Raman spectrum of Dicamba. This process was executed in that same manner and with the same level of theory as the calculations done for the systems only containing Dicamba molecules. As mentioned prior, there are no experimental results in which to compare theoretical results. Comparison and agreement discussions will on be made about the varying positions and number of water molecules. The first discussions will focus on the systems containing one water molecule in different positions and then continue discussing systems as the number of water molecules increases numerically. These discussions will include the hypothesized system to be the most stable based on relative energies. The relatives energies discussed will be in units of kcal/mol. The various combinations of water molecules are depicted by the following images, which were constructed using the program Molekel.

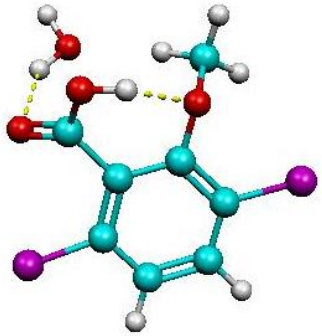

Figure 4B.1

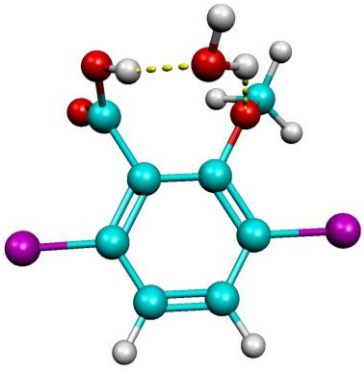

Figure 4B.2

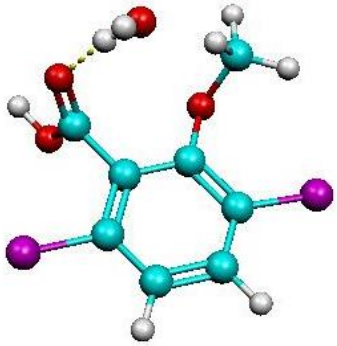

Figure 4B.3

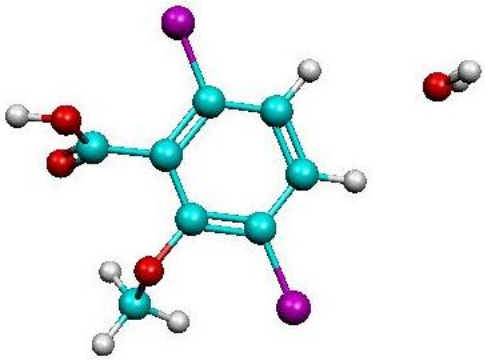

Figure 4B.4

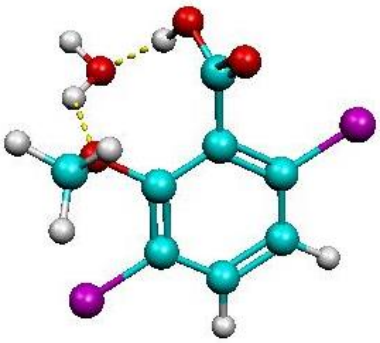

Figure 4B.5

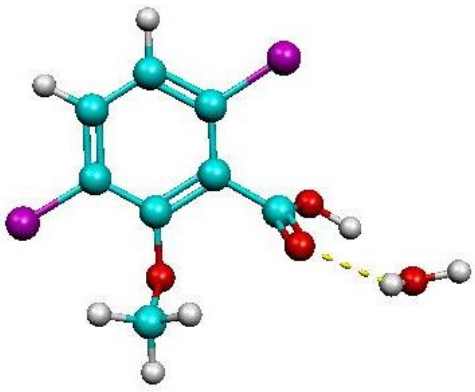

Figure 4B.6

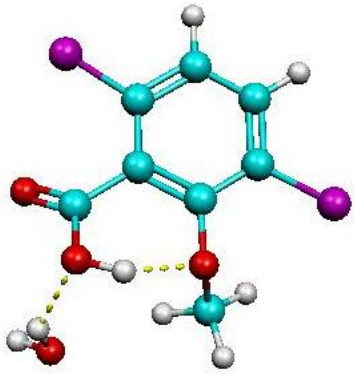

Figure 4B.7

The first simulated water system to be analyzed is that of **Figure 4B.1**. This system contains one water molecule forming a hydrogen bond with the carbonyl. This Raman spectra for this system is shown in **Figure 4.11**. The main shift in vibrational energy modes are seen in the peaks corresponding to carbonyl stretching and O-H stretching. The carbonyl stretching vibrational peak has an energy of 1800.10 cm^{-1} while the O-H stretching peak has an energy of 3620.87 cm^{-1}. With the addition of the one water molecule, both of these vibrational modes experienced a red shift in comparison to the Raman spectrum of the lone Dicamba molecule. A red shift is the lower of energy of a vibrational mode due to a change within the system.

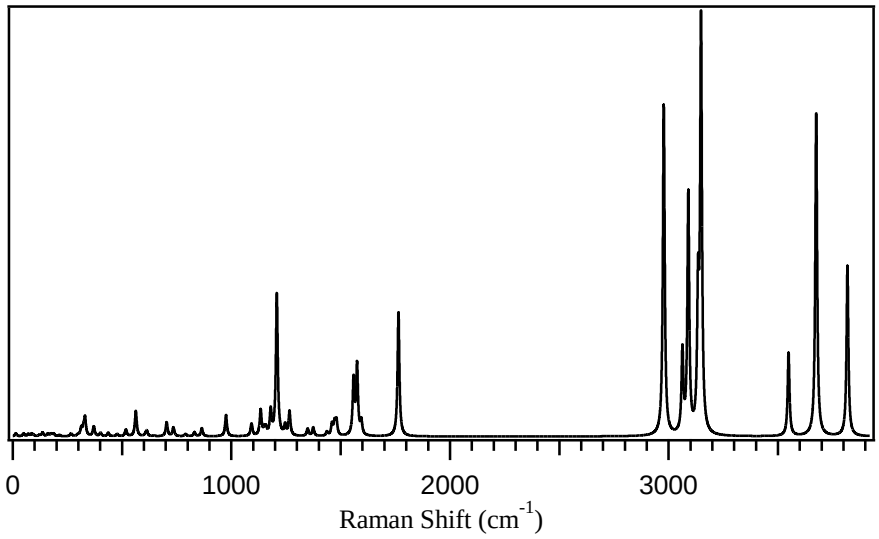

Figure 4.11: Simulated Raman spectra for **Figure 4B.1**.

This decreasing trend for these two vibrational modes is consistent throughout all singular water molecule systems except for two instances. All placements of the one water molecule experience a lowering of energy for the carbonyl stretch vibrational mode. The two exceptions for the O-H stretch vibrational mode occur in the placements of water seen in **Figure 4B.3** and **Figure 4B.4**. These two vibrational modes experience a blue shift, which is the opposite of a red shift and is an increase in energy. One speculation for this increase in energy is that the placement of the water molecule does not impact the O-H functional group. This lack of interaction with the O-H group results in the blue shift for the vibrational mode because the remaining peaks are oppositely affected by the water and experience a red shift. The values for the carbonyl and O-H vibrational modes are shown in **Table 4.1**. In addition, the Raman spectra for the remaining seven configurations follow **Table 4.1**.

Figure	Carbonyl Stretch Energy (cm^{-1})	O-H Stretch Energy (cm^{-1})
4B.1	1800.10	3620.87
4B.2	1814.43	3446.67
4B.3	1786.91	**3736.14**
4B.4	1802.36	**3744.04**
4B.5	1813.91	3441.26
4B.6	1760.89	3359.38
4B.7	1820.95	3553.19

Table 4.1: The table above shows the vibrational modes for the carbonyl and O-H stretch vibrational modes for the one-water molecule systems. The bolded energies are those in which have a greater energy value than vibrational mode value for the Dicamba molecule Raman spectrum.

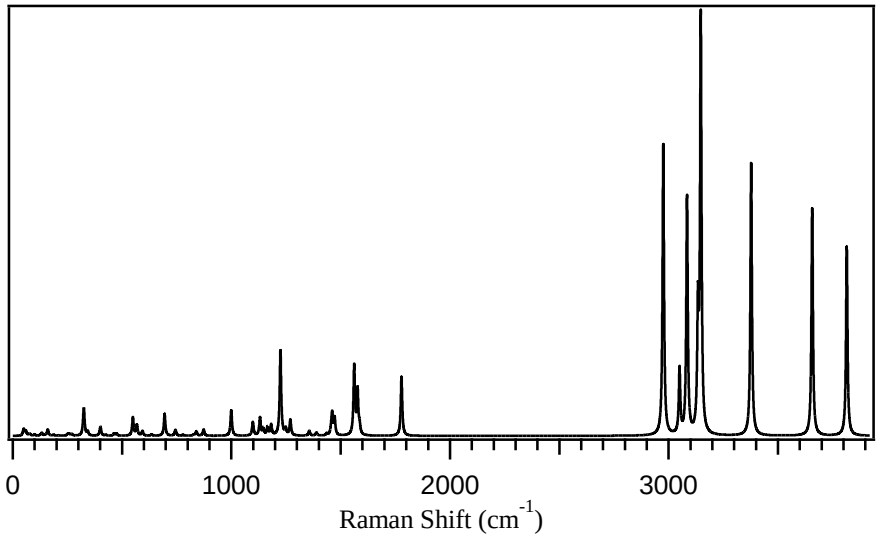

Figure 4.12: Simulated Raman spectra for **Figure 4B.2**.

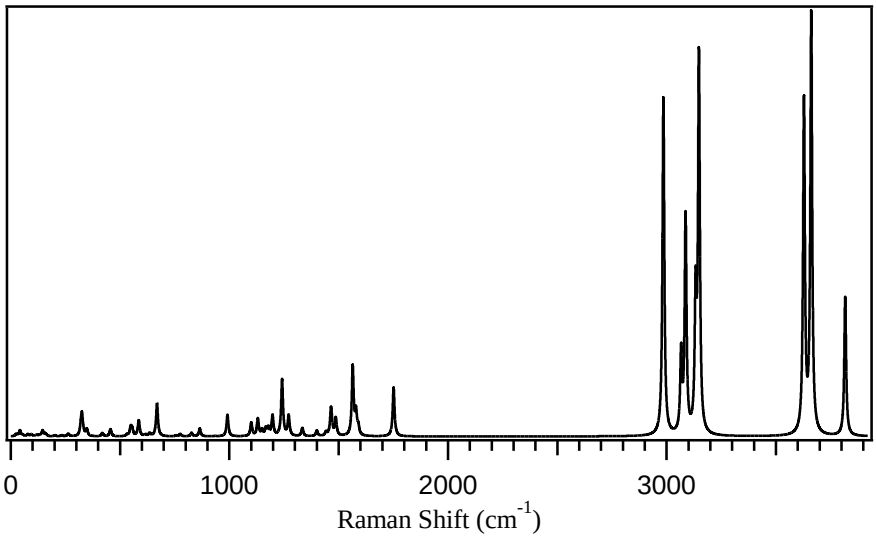

Figure 4.13: Simulated Raman spectra for **Figure 4B.3**.

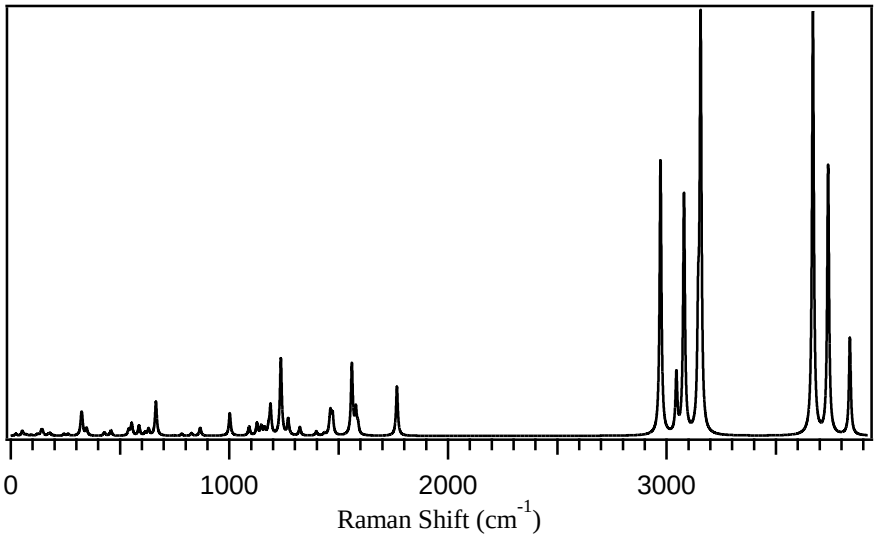

Figure 4.14: Simulated Raman spectra for **Figure 4B.4**.

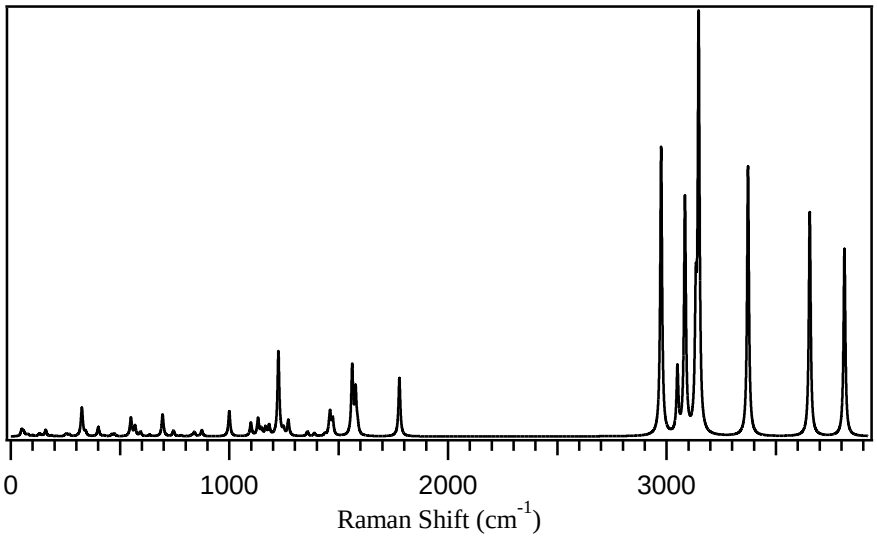

Figure 4.15: Simulated Raman spectra for **Figure 4B.5**.

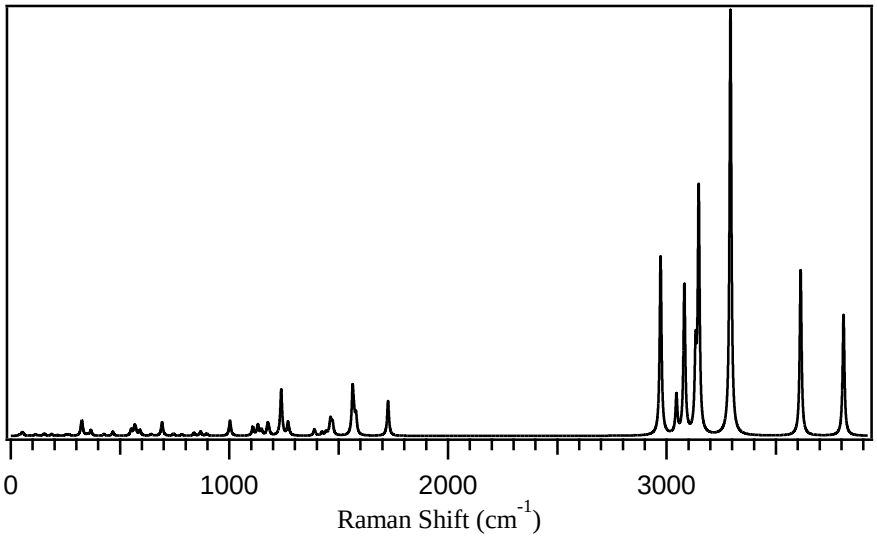

Figure 4.16: Simulated Raman spectra for **Figure 4B.6**.

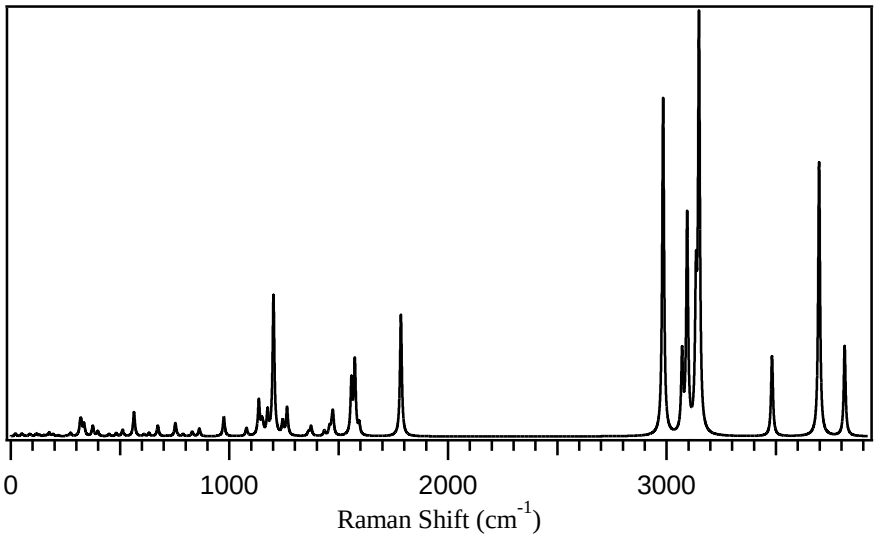

Figure 4.17: Simulated Raman spectra for **Figure 4B.7.**

The final analysis of the one-water systems is the determination of the lowest-energy structure. This was done by taking the value found in the output file. This value is measured in Hartrees. It was converted to kcal/mol using the conversion factor 1 Hartree is equal to 627.5 kcal/mol. The relative energies for the structures studied are shown in **Table 4.2.**

Figure	Relative Energy (kcal/mol)
Figure 4B.1	6.95
Figure 4B.2	3.80
Figure 4B.3	4.74
Figure 4B.4	7.45
Figure 4B.5	3.80
Figure 4B.6	--
Figure 4B.7	7.46

Table 4.2: This table shows the relative energy in kcal/mol for each one-water system. Figure 4B.6 has the lowest energy, making it the most stable.

Looking at **Table 4.2**, the lowest-energy structure is **Figure 4B.6**. The predicted conformation of the one-water system to be the lowest-energy structure was one that resembled **Figure 4B.5**. This figure displays the water molecule forming two hydrogen bonds with the Dicamba molecule. It would be predicted that the formation of two hydrogen bonds would more stabilize the system than only one hydrogen bond formed between the water and Dicamba molecule. Another structure that would have been predicted to have be the lowest-energy structure would be one in which the water molecule forms a hydrogen bond with the Dicamba molecule in addition to the Dicamba molecule also forming a hydrogen bond with itself, which would resemble a structure such as **Figure 4B.1** and **Figure 4B.7**. The same logic as the previous predicted lowest energy structure applies to these figures as well. Further calculations needs to be conducted to corroborate the current data. Since these further calculations cannot be conducted, **Figure 4B.6** will still be the lowest-energy structure for the theoretical one-water systems. The lowest-energy structure for the one-water system will be used in further comparison when the lowest-energy structures for additional water systems are determined.

Simulated Dicamba Spectra: Two Water Molecules

The same steps used for the one-water systems were also used for the two-water systems. The same level of theory, B3LYP and 6-311++G(*d*,*p*), was used. The same analysis was done for the two-water system as well. The carbonyl and O-H stretch vibrational modes were the ones of most interest. In addition, the lowest-energy structure was identified by looking at the energies calculated from the Gaussian16 program. The same conversion factor was used to convert from Hartrees to kcal/mol. The various water

combinations are shown in the following figures. After these figures, the simulated Raman spectra for each configuration is shown. Then the carbonyl and O-H stretch vibrational mode energies are shown in **Table 4.3**.

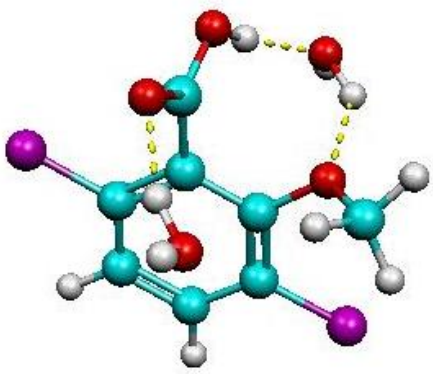

Figure 4B.8

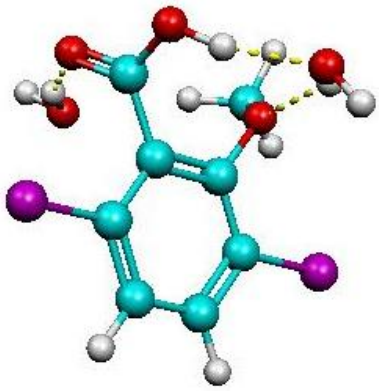

Figure 4B.9

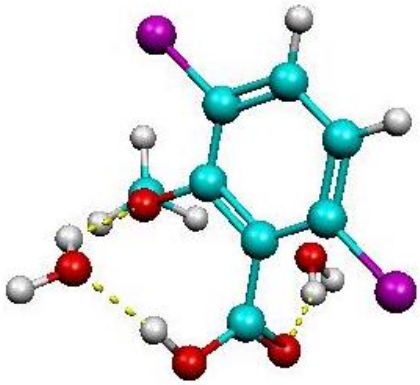

Figure 4B.10

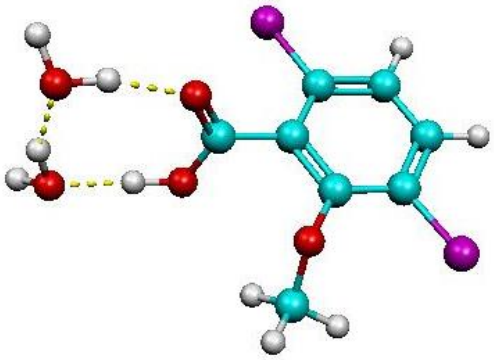

Figure 4B.11

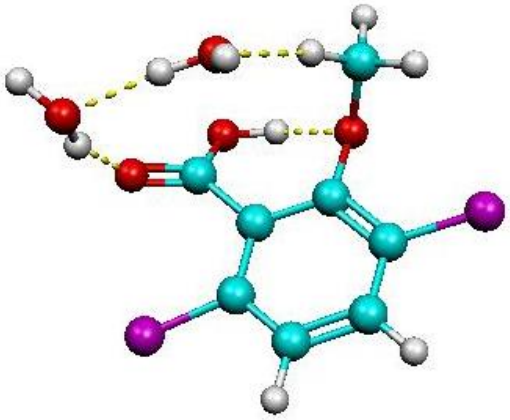

Figure 4B.12

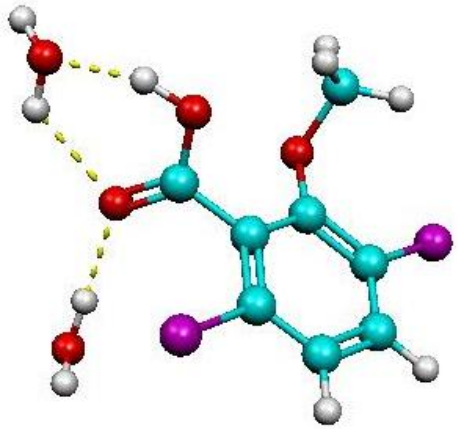

Figure 4B.13

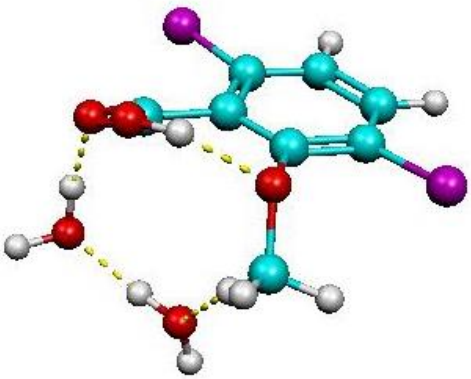

Figure 4B.14

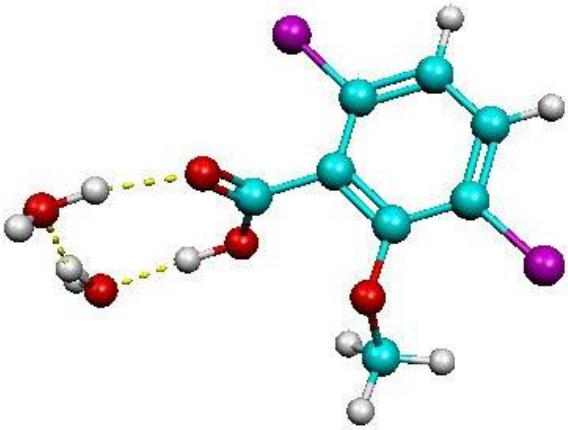

Figure 4B.15

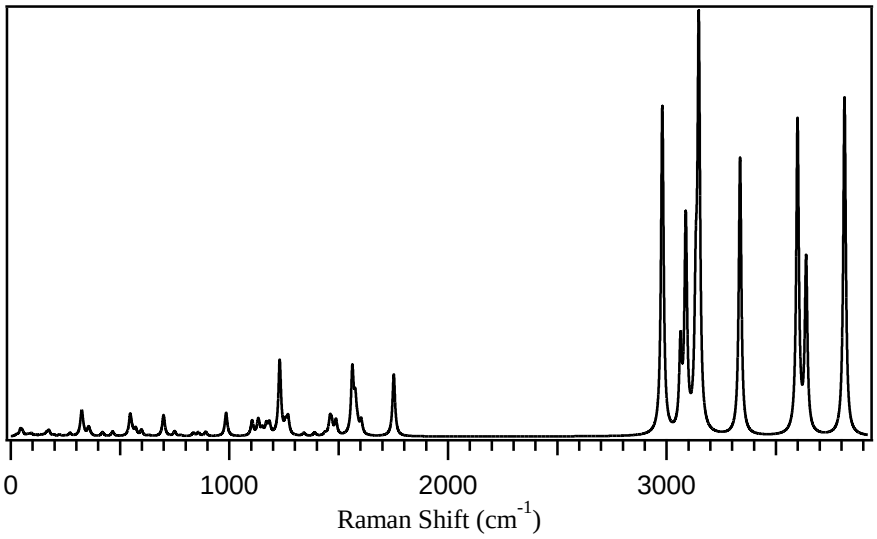

Figure 4.18: Simulated Raman spectrum **Figure 4B.8**.

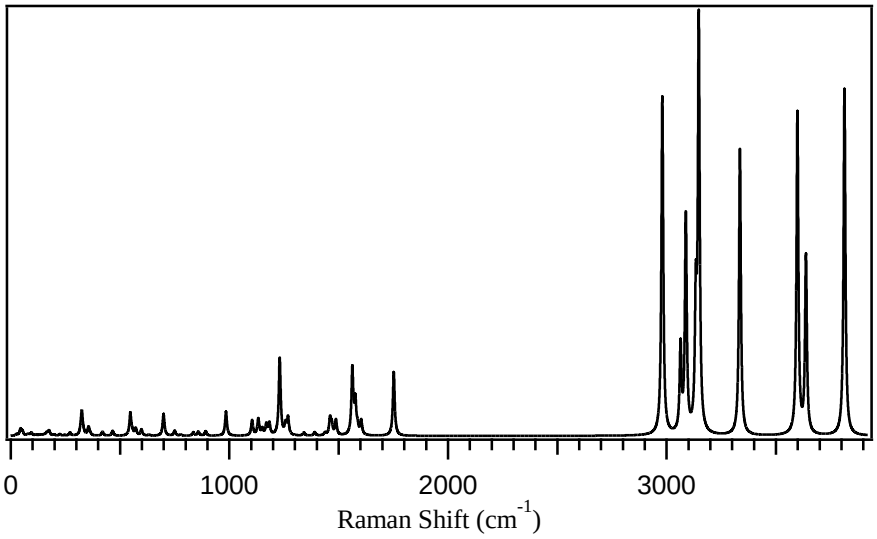

Figure 4.19: Simulated Raman spectrum **Figure 4B.9**.

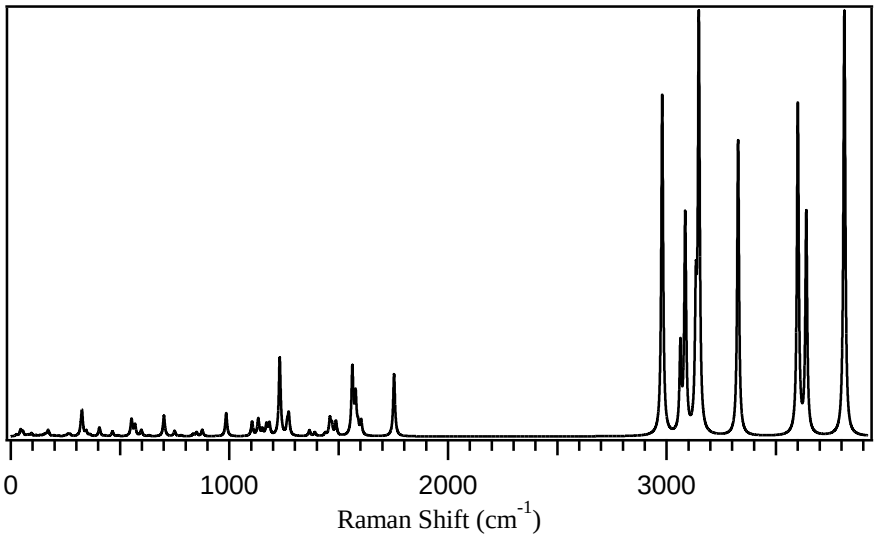

Figure 4.20: Simulated Raman spectrum **Figure 4B.10**.

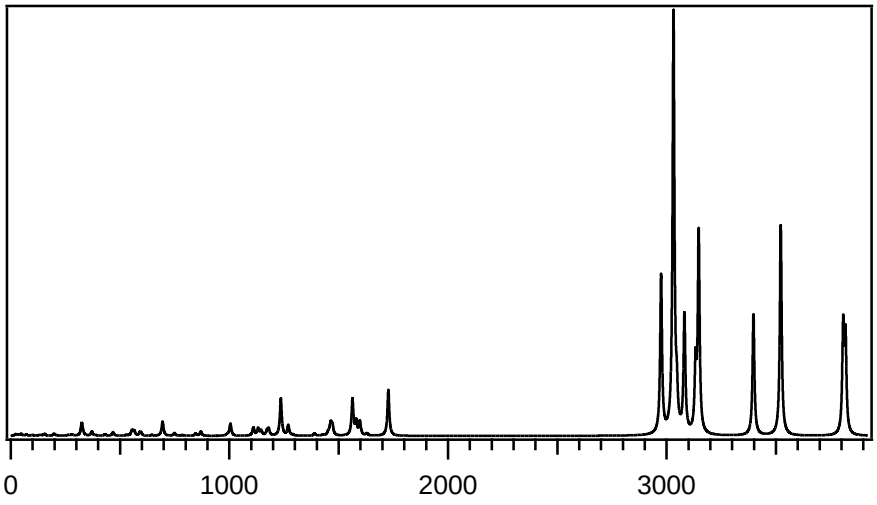

Figure 4.21: Simulated Raman spectrum **Figure 4B.11**.

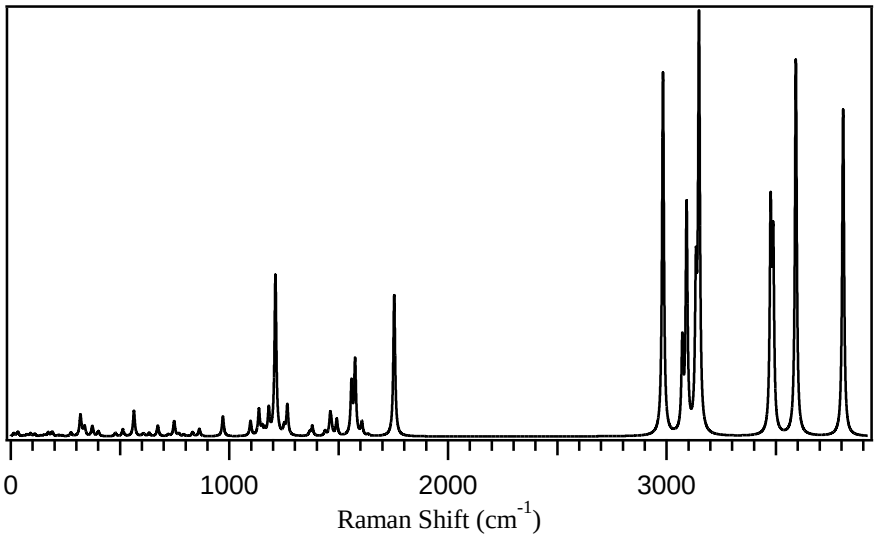

Figure 4.22: Simulated Raman spectrum **Figure 4B.12**.

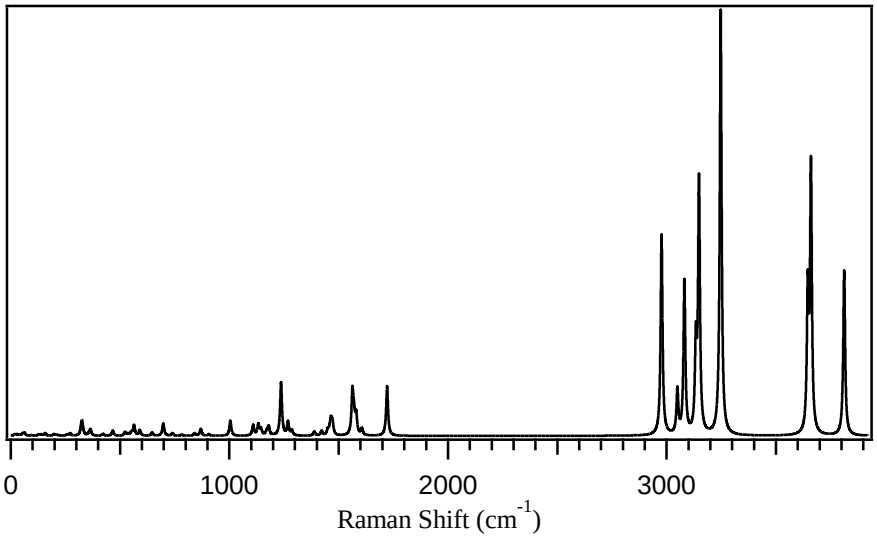

Figure 4.23: Simulated Raman spectrum **Figure 4B.13**.

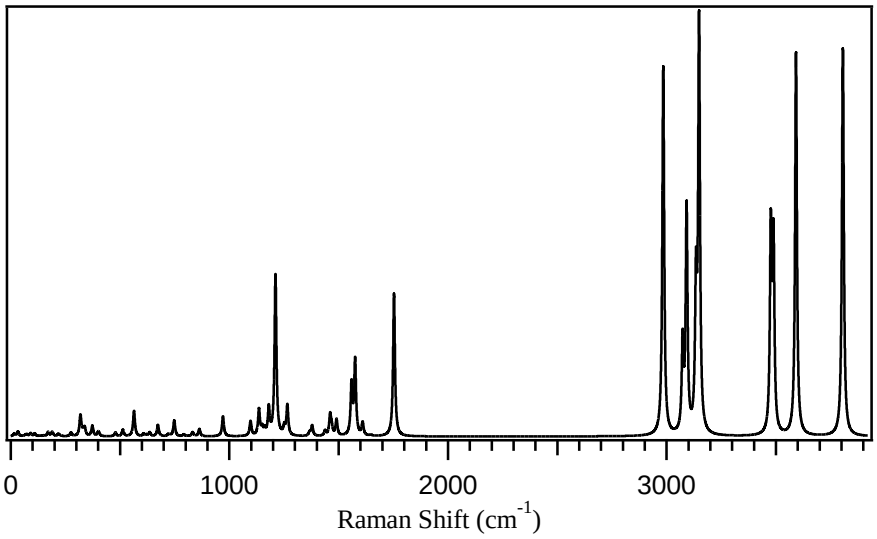

Figure 4.24: Simulated Raman spectrum **Figure 4B.14**.

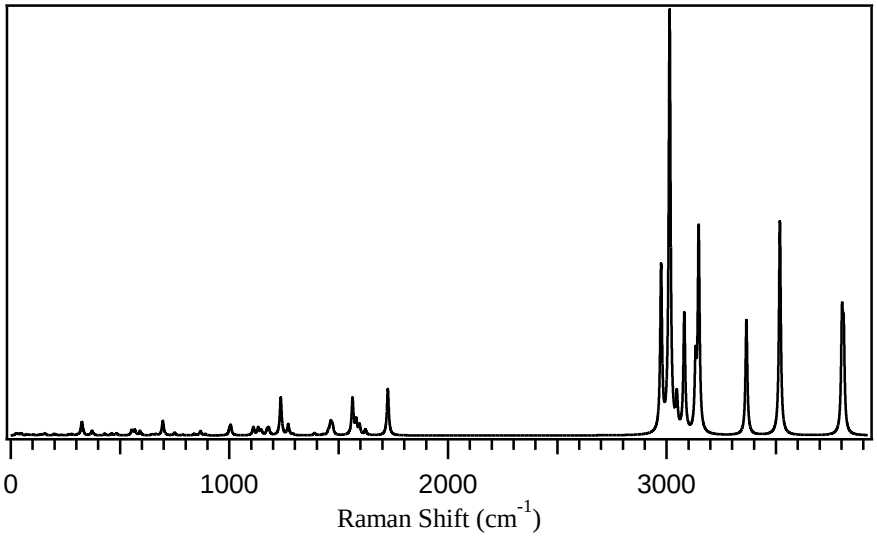

Figure 4.25: Simulated Raman spectrum **Figure 4B.15**.

Figure	Carbonyl Stretch Energy (cm^{-1})	O-H Stretch Energy (cm^{-1})
4B.8	1787.68	3404.23
4B.9	1787.70	3403.53
4B.10	1789.07	3394.98
4B.11	1762.31	3466.70
4B.12	1789.71	3547.00
4B.13	1756.45	3313.68
4B.14	1788.78	3547.69
4B.15	1759.96	3433.82

Table 4.3: The table above shows the vibrational modes for the carbonyl and O-H stretch vibrational modes for the two-water molecule systems. There are no bolded vibrational mode energies in this table because none of the vibrational modes have energies greater than those in the simulated Dicamba spectrum.

The vibrational modes for the carbonyl and O-H stretches on the Raman spectra for the two-water systems are shown in **Table 4.3**. The energies in this table were contrasted with the vibrational mode energies from the singular Dicamba molecule system. For reference, the carbonyl stretch has an energy of 1824.53 cm^{-1} and the O-H stretch vibrational mode has an energy of 3649.33 cm^{-1}. After collecting the vibrational modes for all the two-water theoretical systems, the energies for all vibrational modes were calculated by the Gaussian16 program to be lower than in energy than those of the Dicamba system. This means that the addition of at least two water molecules causes the vibrational modes for the carbonyl and O-H stretches of Dicamba to experience a red shift, or a lowering in energy. The vibrational modes for the O-H stretches display a wide variation in energy. This is due to the more possibilities for hydrogen bonding that can occur at this functional

group. In contrast, among the carbonyl stretch vibrational mode, there is no one theoretical system that is an outlier closest to the vibrational mode of the theoretical Dicamba. The main reason for this lack of deviation among the carbonyl stretch vibrational modes is that there are not as many variations with the carbonyl functional group as seen with the O-H functional group. Only one theoretical instance displays the carbonyl forming two hydrogen bonds, unlike the O-H group, which has many. The only differences among the theoretical systems regarding the carbonyl group is the orientation and placement of water molecules and the Dicamba molecule's functional groups. These difference are not significant enough to result in drastic changes in vibrational mode energy for the carbonyl stretch.

Just like the one-water theoretical systems, the lowest-energy structure was determined. **Table 4.4** shows the overall energies for all nine theoretical two-water systems. As noted in the table, the lowest-energy structure is **Figure 4B.15**. The main speculation for this structure being the lowest-energy of the two-water systems is that both the carbonyl and O-H functional groups are stabilized by the hydrogen bonds formed with the water molecules, and the water molecules also stabilize one another by also forming a hydrogen bond with each other. Having this cyclical ring structure being formed with the water molecules allows for electron density of the carboxylic acid group to be shared with the waters, which causes more stabilizing effects than waters placed in positions that prevent cyclical hydrogen bonding ring formations. **Figure 4B.11** has the smallest relative energy, as shown on **Table 4.4**. When comparing this structure to that of **Figure 4B.15**, there are not many differences that can be pointed out. The reason in which **Figure 4B.11**

has a slightly higher relative energy is that the orientation of the hydrogens and hydrogen bonds is flipped and is not as favorable as that of **Figure 4B.15**.

Figure	Relative Energy (kcal/mol)
4B.8	9.04
4B.9	9.04
4B.10	8.81
4B.11	0.60
4B.12	9.23
4B.13	7.56
4B.14	9.39
4B.15	--

Table 4.4: This table shows the relative energy in kcal/mol for each two-water system. The lowest-energy structure is **Figure 4B.15**.

Simulated Dicamba Spectra: One Dicamba and Three and Four Water Molecules

The last set of results for this project includes a simulated Raman spectrum containing Dicamba with three water molecules and a simulated Raman spectrum of Dicamba with four water molecules. The same steps were followed as previous result sections containing Dicamba and water molecules. The level of theory used was B3LYP and 6-311++G(*d*,*p*). Once the theoretical spectra were obtained, the vibrational modes were assessed and compared to other simulated Raman spectra. Unlike the theoretical combinations for one and two-water systems, the lowest-energy combination can be not determined because not all possible water placements were exhausted. This is a step that will be worked on in future works. At the moment, only one Raman spectrum is available

for three and four water systems **Figure 4B.17** and **Figure 4B.18** show the simulated structures containing three water molecules and four water molecules, respectively. Following these structures are the Raman spectra for these simulated systems and the vibrational modes for the carbonyl and O-H stretches.

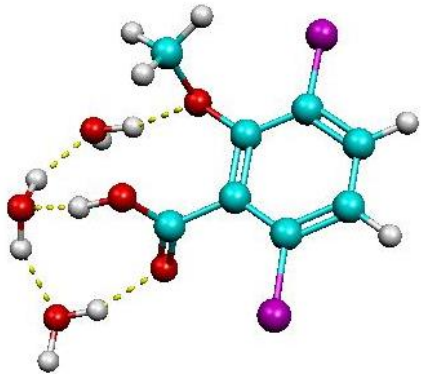

Figure 4B.16

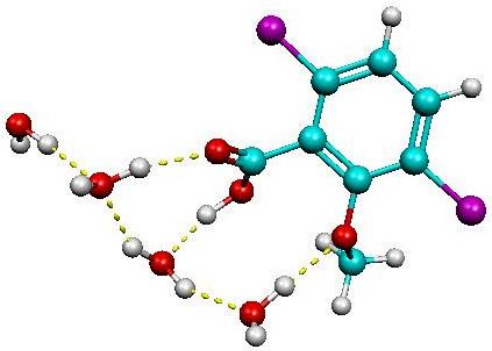

Figure 4B.17

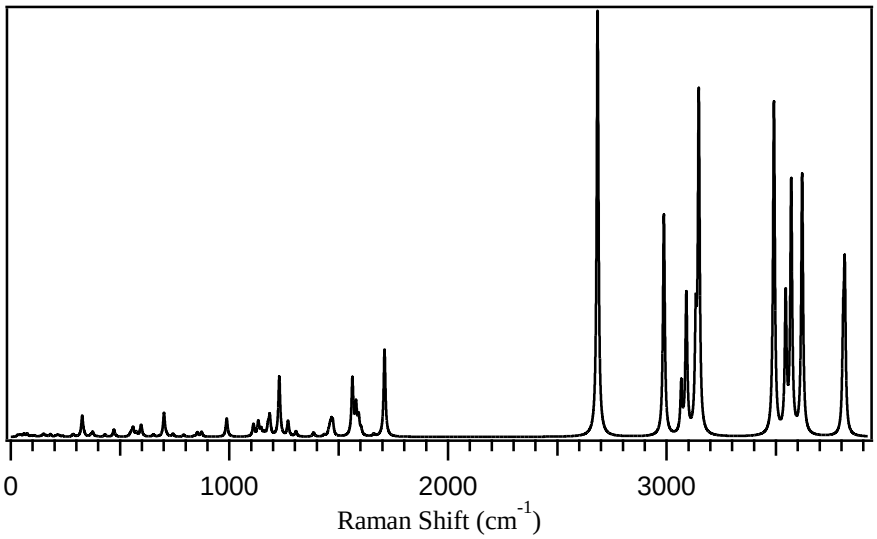

Figure 4.26: Simulated Raman spectrum **Figure 4B.16**.

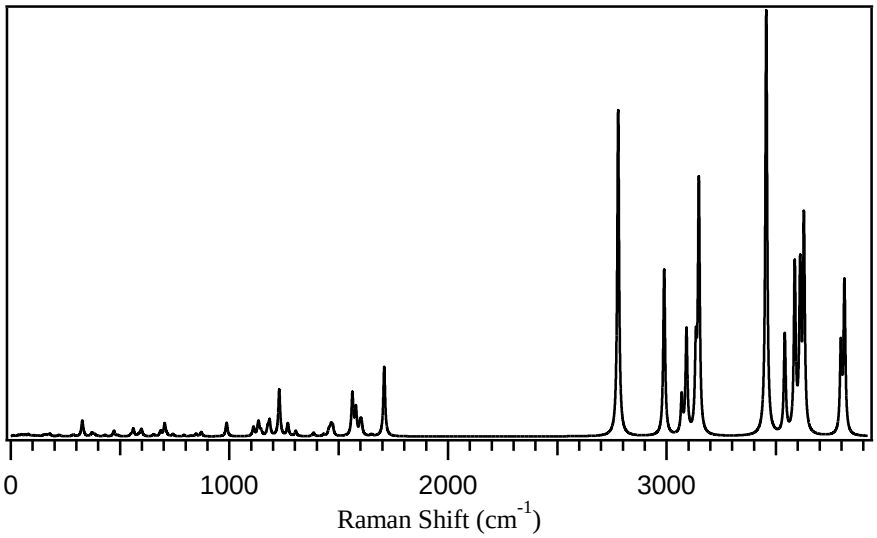

Figure 4.27: Simulated Raman spectrum **Figure 4B.17**.

Just like in previous results sections, the vibrational modes of interest are the carbonyl and O-H stretches. The energies for these vibrational modes for the three and four water systems are shown in **Table 4.5**. These vibrational modes, just like those of the two-water systems, all display a red shift. All vibrational mode energies decreased with the addition of more water molecules. Again for reference, the Dicamba molecule carbonyl stretch was at 1824.53 cm^{-1} and the O-H stretch for this system is at 3649.33 cm^{-1}. The same reasoning for the red shifts seen in these vibrational modes for the two-water systems apply to these systems as well. The additional water molecules stabilize the functional groups and results in decreases in the peaks' energies.

Figure	**Carbonyl Stretch Energy (cm^{-1})**	**O-H Stretch Energy (cm^{-1})**
Figure 4B.16	1744.86	3561.98
Figure 4B.17	1743.15	3526.41

Table 4.5: The table above shows the vibrational modes for the carbonyl and O-H stretches of the three and four-water simulated Raman spectra.

Looking at the energies of these vibrational modes, there is not much difference between these two sets. One reason for this can be due to similar placement of the water molecules. The two simulated environments contain the same configuration of three water molecules. The only difference is the addition of the fourth water molecule in **Figure 4B.17**, which does not interact directly with any part of the Dicamba molecule. Future configurations will include four water molecules that directly interact with the Dicamba molecule.

The next comparison made in the project compares the three and four-water systems. The reasoning for the similar values for the vibrational modes has already been addressed. Looking the spectra side-by-side, there are not many differences to be addressed. The only noticeable differences to be mentioned is the additional peaks seen in the four-water system. One of the most intense of these additional peaks includes the O-H stretch of a water molecule at 2834.97 cm^{-1} of the four-water spectra. Peaks such as these are expected because new vibrational modes are added with the addition of each new water molecule. This comparison can be seen in **Figure 4.28**.

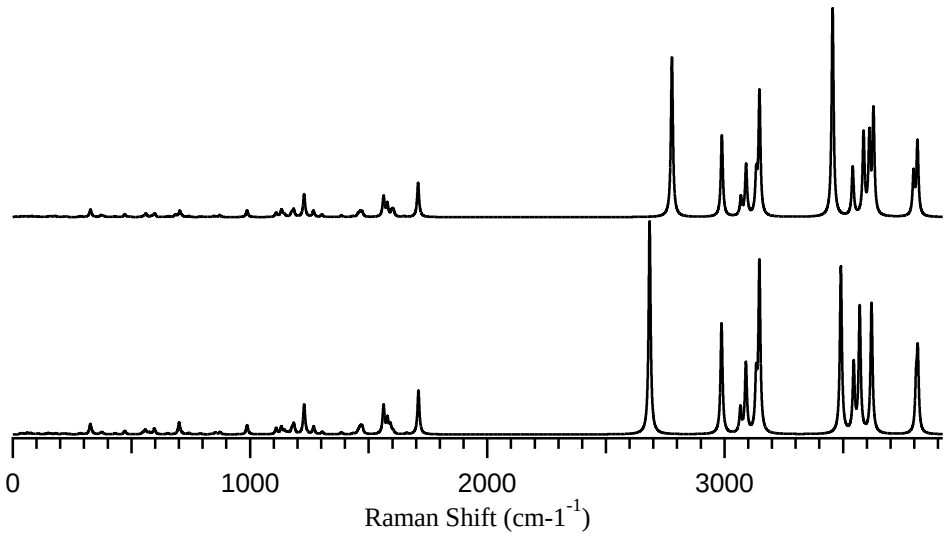

Figure 4.28: Comparison of three and four-water systems. The three-water system is shown on the bottom.

Simulated Dicamba Spectra: Comparison Between Dicamba and Water Combinations

The next comparison to be made in this project is among the lone Dicamba molecule, the lowest-energy structures for one and two-water molecule systems, and the three and four-water systems. Though the three and four-water systems are not the guaranteed lowest-energy structure for the specific number of water molecules, the comparison of all these systems will still provide insight to the impact of adding water molecules to a Dicamba molecule. **Figure 4.29** shows this comparison.

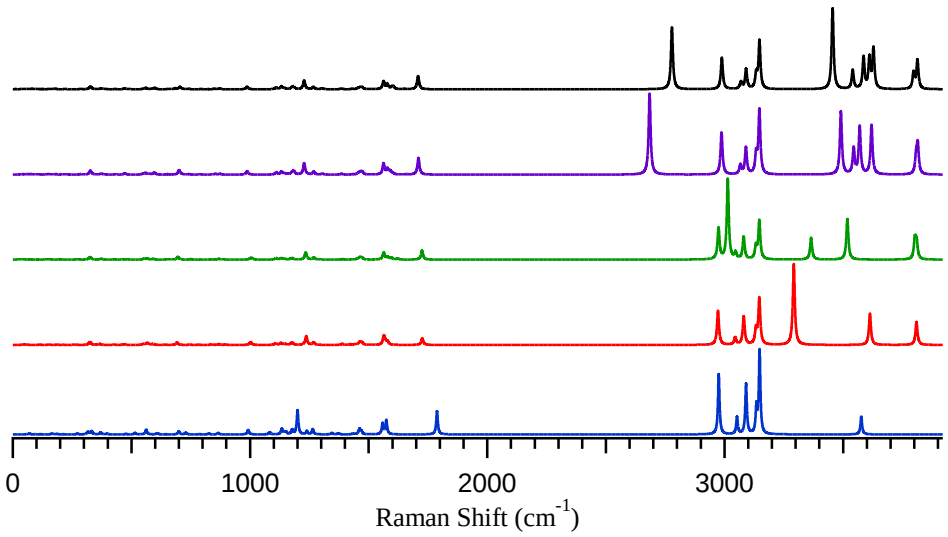

Figure 4.29: Comparison of Raman spectra for the one Dicamba molecule (blue), the lowest-energy structures of the one (red) and two-water systems (green), three-water system (purple), and four-water system (black).

At first glance, there are various differences among the five theoretical spectra. The most prominent differences are those that have been mentioned throughout the entire results section. The addition of water molecules results in the shift of both the carbonyl and O-H peaks. This, again, is due to the stabilizing effects of hydrogen bond formation due to the water molecule addition. In addition, more peaks are seen as more water molecules are added because vibrational modes are added for each new water. These shifts can be seen in **Figure 4.30** and **Figure 4.31**, which focuses on the carbonyl and O-H stretch vibrational modes, respectively.

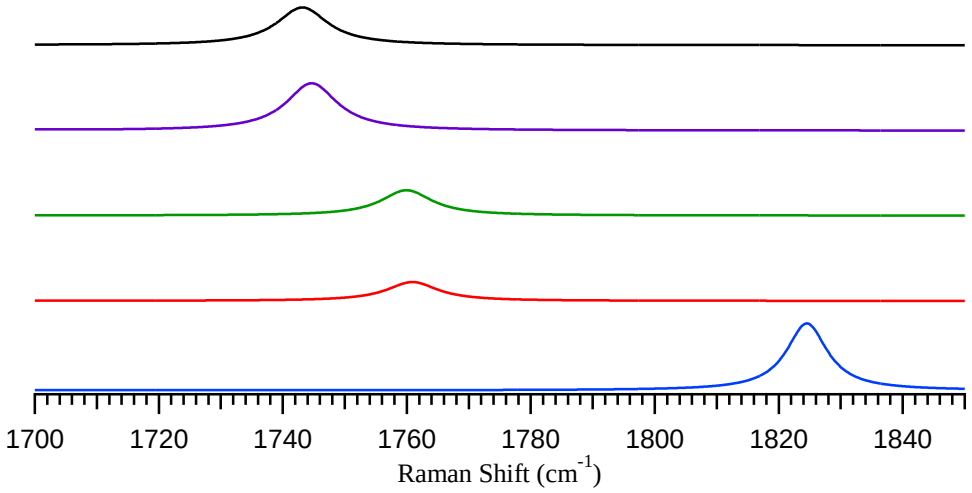

Figure 4.30: Focused look of the carbonyl stretch vibrational for the comparison made in **Figure 4.29**.

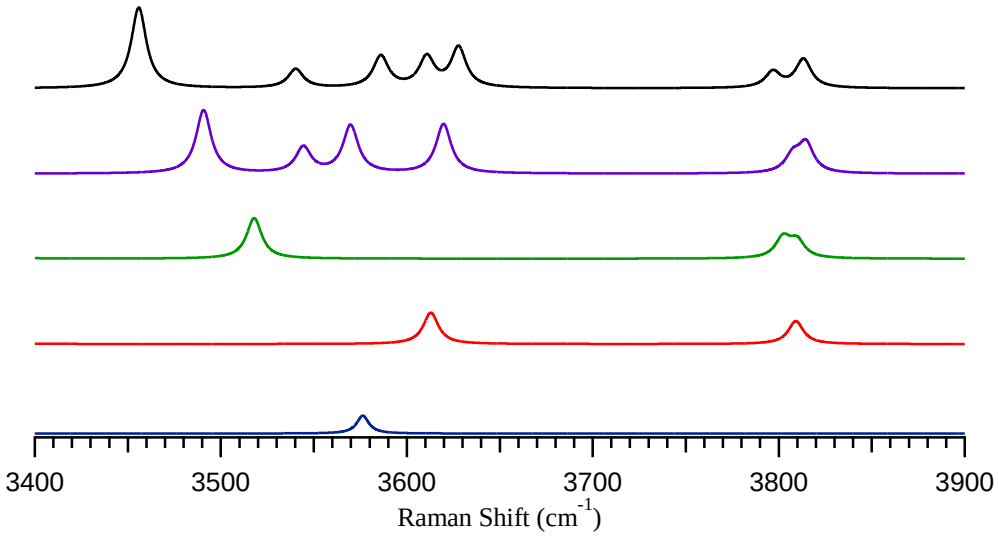

Figure 4:31: Focused look of the O-H stretch vibrational for the comparison made in **Figure 4.29**.

The final comparison of this project replaces the one Dicamba system for the crystal structure database dimer simulated system. This spectrum was chosen over the optimized dimer system because the crystal structure dimer system has more intense peaks and a more optimized geometry. This comparison can be seen in **Figure 4.32**.

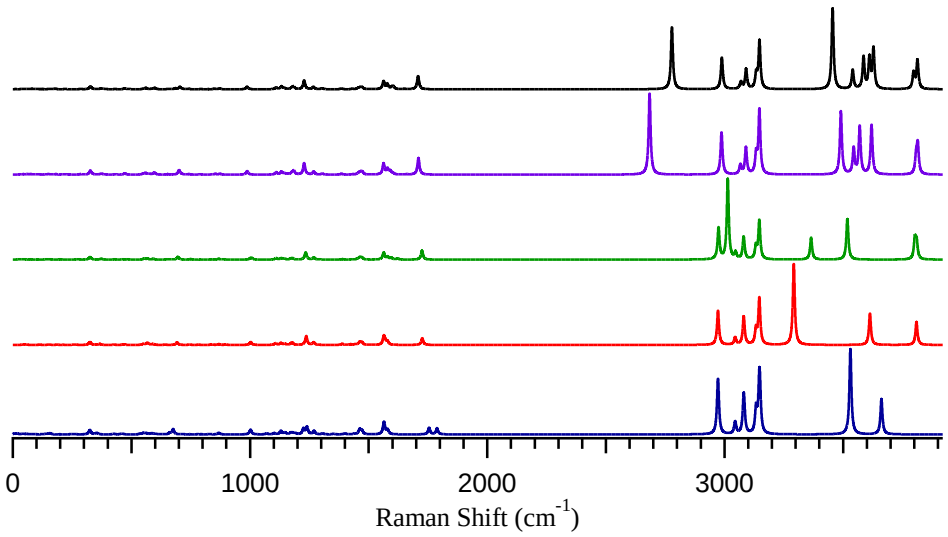

Figure 4.32: Comparison of Raman spectra for the dimer system (blue), the lowest-energy structures of the one (red) and two-water systems (green), three-water system (purple), and four-water system (black).

The most significant difference among these spectra is that the dimer system spectrum's carbonyl and O-H stretches have at least one higher energy than those containing water. This is an expected trend because the water molecules interact directly with the carbonyl and O-H functional groups, acting as stabilizing factors for these vibrational modes. In contrast, the interactions within the dimer do not directly stabilize the functional groups to the degree in which the water molecules do, which is why the carbonyl and O-H vibrational modes have higher energy in the dimer system. A more focused view for these vibrational mode shifts can be seen in **Figure 4.34** and **Figure 4.34**.

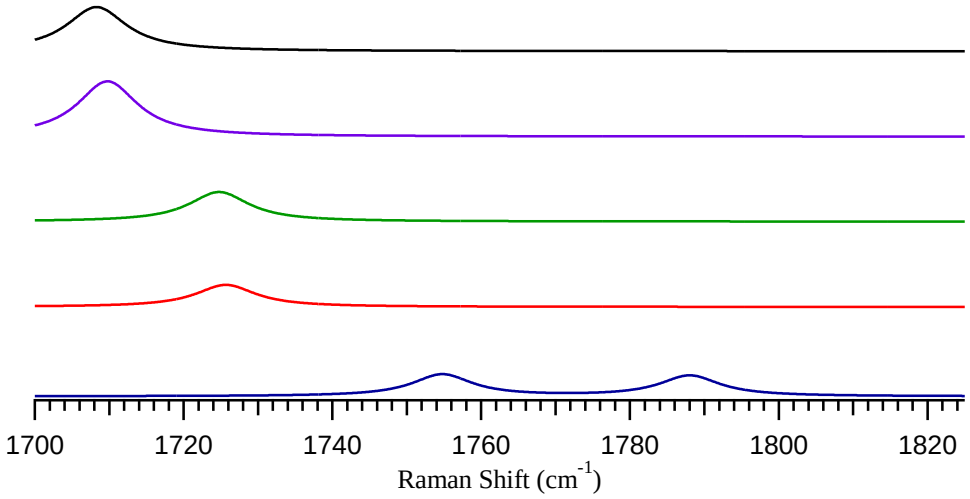

Figure 4.33: Focused look of the carbonyl stretch vibrational for the comparison made in **Figure 4.32**.

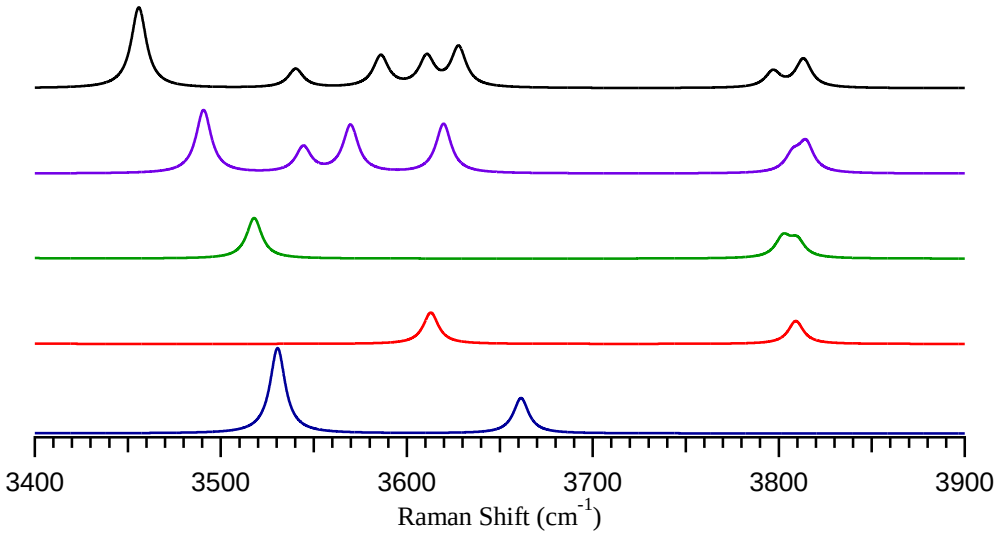

Figure 4:34: Focused look of the O-H stretch vibrational for the comparison made in **Figure 4.32**.

Chapter 5: Summary and Future Works

Dicamba's recent appearances in headlines have made it more necessary than ever to have mechanisms and techniques in place to identify Dicamba in an environmental and agricultural setting. One of these mechanisms used to identify Dicamba in a real-world situation can be Raman spectroscopy. Handheld Raman spectrometers have been used as instruments for forensic chemistry studies but have slowly transitioned into other sectors of industry such as agriculture. The ability to identify Dicamba has grown in importance because of the volatility this active ingredient has. Its capability of drifting and causing off-target injuries is an issue the agricultural industry must combat quickly and effectively. The loss of crops to off-target injury means less food is being made for an exponentially growing global population. For these reasons, tools that can identify Dicamba should be accessible. The Raman spectrum for Dicamba has not been identified. Only available spectra for this molecule have been found using Nuclear Magnetic Resonance spectroscopy, Mass Spectrometry, and Infrared spectroscopy. The addition of Raman spectra will only aid in the identification of Dicamba. The mimicked systems in this project were created to simulate instances in which Dicamba would be studied experimentally and found in the environment. The Dicamba dimer systems were created to give greater insight about the crystalline structure of Dicamba powder than an individual Dicamba molecule would have. The simulated calculations containing water were created to provide ways in which to observe the impact of water on a Raman spectrum, which

will prove useful for potential runoff issues with the pesticide. The designation of the lowest-energy structures was done to provide the most optimized geometry for that combination of molecules. Though experimental results would vary from theoretical spectra due to external factors, the lowest-energy spectra provide a reference for any experimental spectra collected or other simulated spectra calculated. The addition of water molecules showed that key vibrational modes, the carbonyl and O-H stretches, displays red shifts. This knowledge can prove to be vital for agricultural research because these simulated systems emulate possible situations in which Dicamba will be found. This is yet another technique that now has the capability of being used to detect Dicamba in real-world situations.

Future works include increasing the amount of Dicamba molecules in a system and also increasing the amount of water molecules as well. This is in hopes of creating systems that closer reflect what would be seen in studied samples from the environment. These systems would most likely require different methods and basis sets to accommodate for the growing systems. In addition, future works would include obtaining more experimental data, which was interrupted by the COVID-19 pandemic. This would include obtaining more accurate spectra of the powder sample of Dicamba and also spectra of Dicamba dissolved in water. These experimental studies would follow the same procedure to acquire data as the experimental data presented in this project. The only variations to occur would be with the water studies, which would require a slightly different setup to contain the sample since it is a liquid.

References:

1. Grube, Arthur, David Donaldson, Timothy Kiely, and La Wu. "Pesticides industry sales and usage." *US EPA, Washington, DC* (2011).
2. O'Donoghue, Erik J., David E. Banker, Robert Ebel, Keith Fuglie, Penni Korb, Michael Livingston, Cynthia Nickerson, and Carmen Sandretto. *The changing organization of US farming*. No. 1476-2019-2784. 2011.
3. Food and Agriculture Organization of the United Nations. 1986. International Code of Conduct on the Distribution and Use of Pesticides. Rome, FAO, 1986.
4. Amdur, M. O., J. Doull, and C. D. Klaassen. "Educational and informational strategies to reduce pesticide risks." *Preventive medicine* 26, no. 2 (1997): 191-200.
5. Das, Shaon Kumar, and Tilak Mondal. "Mode of action of herbicides and recent trends in development: a reappraisal." *Int. J. Agric. Soil Sci* 2 (2014): 27-32.
6. Lévesque, C. André, and James E. Rahe. "Herbicide interactions with fungal root pathogens, with special reference to glyphosate." *Annual Review of Phytopathology* 30, no. 1 (1992): 579-602.
7. Ranga Rao, G. V., O. P. Rupela, V. Rameshwar Rao, and Y. V. R. Reddy. "Role of biopesticides in crop protection: present status and future prospects." *Indian journal of plant protection* 35, no. 1 (2007): 1-9.
8. Miller, G. T. "Living in the environment. Belmont: Wadsworth/Thomson learning." *ISBN o-534-37697-5* (2002).
9. National Research Council. *The future role of pesticides in US agriculture*. National Academies Press, 2000.
10. Hernández Escalona, M., and Fuentes Fiallo. "V, Alfonso Hernández, M., Avilés Pacheco, R. and Isman, M.(2006) Botanical insecticides, deterrents, and repellents in modern agriculture and an increasingly regulated world." *Annual Review of Entomology* 51: 45-66.
11. Chiu, Shin-Foon. "Recent advances in research on botanical insecticides in China." 1989.
12. Dunlap, Thomas. *DDT: scientists, citizens, and public policy*. Princeton University Press, 2014.

13. Chapin, Georganne, and Robert Wasserstrom. "Agricultural production and malaria resurgence in Central America and India." *Nature* 293, no. 5829 (1981): 181-185.
14. Davis, Frederick Rowe. *Banned: a history of pesticides and the science of toxicology*. Yale University Press, 2014.
15. Peacock, F. C. *Jealott's Hill: Fifty years of Agricultural Research: 1928-1978*. 1978.
16. Quastel, J. H. "2, 4-Dichlorophenoxyacetic Acid (2, 4-D) as a selective herbicide." 1950.
17. Ritter, Steven K. "Pinpointing trends in pesticide use." *Chemical and Engineering News* 87, no. 7 (2009).
18. Franz, John E., Michael K. Mao, and James A. Sikorski. *Glyphosate: a unique global herbicide*. American Chemical Society, 1997.
19. Myers, John Peterson, Michael N. Antoniou, Bruce Blumberg, Lynn Carroll, Theo Colborn, Lorne G. Everett, Michael Hansen et al. "Concerns over use of glyphosate-based herbicides and risks associated with exposures: a consensus statement." *Environmental Health* 15, no. 1 (2016): 1-13.
20. Nyamai, Priscilla A., Timothy S. Prather, and John M. Wallace. "Evaluating restoration methods across a range of plant communities dominated by invasive annual grasses to native perennial grasses." *Invasive Plant Science and Management* 4, no. 3 (2011): 306-316.
21. Funke, Todd, Huijong Han, Martha L. Healy-Fried, Markus Fischer, and Ernst Schönbrunn. "Molecular basis for the herbicide resistance of Roundup Ready crops." *Proceedings of the National Academy of Sciences* 103, no. 35 (2006): 13010-13015.
22. Benbrook, Charles M. "Trends in glyphosate herbicide use in the United States and globally." *Environmental Sciences Europe* 28, no. 1 (2016): 3.
23. Dill, Gerald M. "Glyphosate-resistant crops: history, status and future." *Pest Management Science: formerly Pesticide Science* 61, no. 3 (2005): 219-224.
24. Fernandez-Cornejo, Jorge, Seth Wechsler, Mike Livingston, and Lorraine Mitchell. "Genetically engineered crops in the United States." *USDA-ERS Economic Research Report* 162 (2014).
25. Nandula, Vijay K., ed. *Glyphosate resistance in crops and weeds: history, development, and management*. John Wiley & Sons, 2010.
26. Hartzler, Bob. “A historical perspective on dicamba.” (2017).
27. Behrens, Mark R., Nedim Mutlu, Sarbani Chakraborty, Razvan Dumitru, Wen Zhi Jiang, Bradley J. LaVallee, Patricia L. Herman, Thomas E. Clemente, and Donald P. Weeks. "Dicamba resistance: enlarging and preserving biotechnology-based weed management strategies." *Science* 316, no. 5828 (2007): 1185-1188.

a. Dicamba resistance

28. United States Department of Agriculture, "Monsanto Petitions (10-188-01p and 12-185-01p) for Determinations of Nonregulated Status for Dicamba-Resistant Soybean and Cotton Varieties: Final Environmental Impact Statement," December 2014.
29. Brook, Charles. *Dicamba Diary Part I: Discovery and Development*. 2017.
30. Egan, J. Franklin, Kathryn M. Barlow, and David A. Mortensen. "A meta-analysis on the effects of 2, 4-D and dicamba drift on soybean and cotton." *Weed Science* 62, no. 1 (2014): 193-206.
31. Mortensen, David A., J. Franklin Egan, Bruce D. Maxwell, Matthew R. Ryan, and Richard G. Smith. "Navigating a critical juncture for sustainable weed management." *BioScience* 62, no. 1 (2012): 75-84.
32. Wang, Magnus, and Dirk Rautmann. "A simple probabilistic estimation of spray drift—factors determining spray drift and development of a model." *Environmental Toxicology and Chemistry: An International Journal* 27, no. 12 (2008): 2617-2626.
33. Boerboom, Chris. "Field case studies of dicamba movement to soybeans." In *Wisconsin Crop Management Conference: 2004 Proceedings Papers. University of Wisconsin–Madison.(12 October 2011*. 2004.
34. Unglesbee, Emily. "Dicamba Questions. How Often Could Growers Legally Spray Dicamba in 2017?." *DTN Progressive Farmer. Sept* 15 (2017).
35. Sadava, David E., H. Craig Heller, William K. Purves, Gordon H. Orians, and David M. Hillis. *Life: The science of biology*. Macmillan, 2008.
36. Hohm, Tim, Tobias Preuten, and Christian Fankhauser. "Phototropism: translating light into directional growth." *American journal of botany* 100, no. 1 (2013): 47-59.
37. Benková, Eva, Marta Michniewicz, Michael Sauer, Thomas Teichmann, Daniela Seifertová, Gerd Jürgens, and Jiří Friml. "Local, efflux-dependent auxin gradients as a common module for plant organ formation." *Cell* 115, no. 5 (2003): 591-602.
38. Mano, Yoshihiro, and Keiichirou Nemoto. "The pathway of auxin biosynthesis in plants." *Journal of experimental Botany* 63, no. 8 (2012): 2853-2872.
39. Gleason, Cynthia, Rhonda C. Foley, and Karam B. Singh. "Mutant analysis in Arabidopsis provides insight into the molecular mode of action of the auxinic herbicide dicamba." *PloS one* 6, no. 3 (2011).
40. Grossmann, Klaus. "Auxin herbicides: current status of mechanism and mode of action." *Pest Management Science: formerly Pesticide Science* 66, no. 2 (2010): 113-120.
41. Burg, Stanley P., and Ellen A. Burg. "Role of ethylene in fruit ripening." Plant Physiology 37, no. 2 (1962): 179.

42. Tro, Nivaldo J. Chemistry: A Molecular Approach. 2nd ed. New Jersey: Pearson, 2011. Pearson. Web. 31 Mar. 2017.
43. McHale, Jeanne L. Molecular Spectroscopy. Boca Raton: CRC, 2017. Print.
44. Engel, Thomas, Philip Reid, and Warren Hehre. Physical Chemistry. Boston: Pearson, 2013. Print.
45. Sienerth, Karl D.., Granger, Jill N.., Granger, Robert M.. Instrumental Analysis: Revised Edition. United Kingdom: Oxford University Press, 2017.
46. Nelson, David L., Albert L. Lehninger, and Michael M. Cox. *Lehninger principles of biochemistry*. Macmillan, 2013.